NASA CR-54604
HTL TR NO. 82

SUMMARY REPORT

FILM COOLING WITH INJECTION THROUGH A CIRCULAR HOLE

by

R.J. Goldstein, E.R.G. Eckert and J.W. Ramsey

prepared for

NATIONAL AERONAUTICS AND SPACE ADMINISTRATION

May 14, 1968

CONTRACT NAS 3-7904
TECHNICAL MANAGEMENT
NASA Lewis Research Center
Cleveland, Ohio
Lewis Project Manager; Francis S. Stepka

University of Minnesota
Institute of Technology
Department of Mechanical Engineering
Minneapolis, Minnesota 55455

ABSTRACT

An experimental investigation is reported on the film cooling effectiveness with injection of air through a discrete hole into a turbulent boundary layer of air on a flat plate. The secondary air enters the mainstream through a circular tube inclined at an angle of either 35 degrees or 90 degrees to the main flow. Basic trends are found to be similar for the two injection angles, with differences occurring only at large injection rates. Although the trends are the same for the two injection angles, sizable differences are found in the level of cooling which can be obtained. Injection at an angle of 35 degrees is found to yield higher effectiveness values than 90 degree injection. The film cooling effectiveness for both injection angles is found to be considerably different from that obtained when the secondary fluid is introduced through a continuous slot.

NOMENCLATURE

C	constant of proportionality in Eq. (3)
D	diameter of injection tube
M	blowing rate parameter, $M = \rho_2 U_2 / \rho_\infty U_\infty$
R	radial position in injection tube
Re_D	injection tube Reynolds number, $Re_D = U_2 D / \nu_2$
S	slot height or equivalent slot height
T	temperature
T_{Bulk}	bulk temperature of secondary air
T_{Max}	maximum temperature of secondary air
T_{aw}	adiabatic wall temperature
T_2	temperature of secondary air used in defining η (temperature 4½ - 6 diameters upstream of tube exit)
T_∞	mainstream temperature
U	velocity
U_2	average air velocity in injection tube
U_∞	mainstream velocity
X	distance downstream of injection hole, see Figure 1
X'	distance downstream of boundary layer trip wire
Y	distance normal to tunnel floor, see Figure 1
Z	lateral distance from injection hole, see Figure 1
$Z_{½}$	lateral position at which the film cooling effectiveness parameter is equal to one-half its value at Z equal zero
δ	boundary layer thickness
δ^*	displacement thickness, defined by Eq. (3)

δ_i momentum thickness, defined by Eq. (5)

ν_2 kinematic viscosity of secondary air

ν_∞ kinematic viscosity of mainstream

η film cooling effectiveness parameter, defined by Eq. (6)

ρ density

ρ_2 density of secondary air

ρ_∞ density of mainstream

τ_w wall shear stress

FILM COOLING WITH INJECTION THROUGH A CIRCULAR HOLE

by

R. J. Goldstein, E.R.G. Eckert, and J. W. Ramsey

University of Minnesota

I. SUMMARY

The study described in this summary report was carried out under NASA Contract NAS 3-7904. It is an experimental investigation to determine the film cooling effectiveness obtained by injection of heated air through a discrete hole into a turbulent boundary layer of air on a flat plate.

A subsonic wind tunnel was constructed especially for the studies reported herein. The tunnel is designed to ensure good flow quality in the test section. (i.e. uniformity of the velocity field, low turbulence level, flow steadiness and absence of swirl.) The test section of the tunnel is designed so that local adiabatic wall temperatures can be measured downstream of the position at which the heated secondary gas is introduced into the tunnel. Since local adiabatic-wall temperature measurements are desired, special care is taken to ensure that the wall has negligible conduction parallel to its surface in addition to being well insulated in a direction normal to its surface.

Adiabatic-wall temperature measurements are obtained for two different injection angles. The secondary air enters through a 2.35 cm diameter tube inclined at an angle of either 35 degrees or 90 degrees to the main flow. For each of these inclinations, temperature distributions are measured for two mainstream velocities, 30.5 m/sec and 61 m/sec. The ratio of the mass flux of the injected gas to the mass flux of the freestream covered in the investigation is between 0.1 and 2.0. In all of the experiments the secondary gas is injected at a temperature approximately 55^{o}C higher that that of the mainstream. When the injected air enters at an angle of 90^{o} to the mainstream it encounters a turbulent boundary layer whose displacement thickness is approximately 0.09 cm. The displacement thickness for 35^{o} injection is approximately 0.14 cm at the injection location.

Basic trends are found to be similar for the two injection angles with difference occuring only at large injection rates. Although the trends are the same for the two angles of injection, sizable differences are found in the level of cooling which can be obtained. Injection at an angle of 35 degrees is found to yield higher effectiveness values than 90 degree injection. The film cooling effectiveness for both injection angles is found to be considerably different from that obtained when the secondary fluid is introduced through a continuous slot.

II. INTRODUCTION

Film cooling is used extensively in recent technological applications as a means to protect various structural elements against the influence of a hot gas stream. In this method, a coolant (liquid or gas) is ejected locally through the wall of the structure to be protected, in such a way that it creates a film along the wall which protects the structure from the influence of the hot fluid. The gas, which will be considered as coolant, in this discussion is ejected through a continuous slot, or strip of porous material, or through an arrangement of shorter openings in single or multiple rows.

Film cooling with injection through a continuous slot or a porous strip has been investigated in the greatest detail. This is natural because the flow and temperature fields downstream of the slot are two-dimensional and in this way the investigation, which is already made difficult by the large number of parameters involved, is simplified. In several experimental studies, near tangential injection has been used (1, 2, 3).*

---

*Underlined numbers in parentheses designate References at end of paper.

Other investigations (4, 5) employ a step-down slot to introduce the secondary gas. Film cooling experiments have also been reported with air (6, 7) and helium (8) injected through a porous strip. A number of authors (9, 10, 11, 12) presented semi-analytical predictions of film cooling with a turbulent boundary layer.

Continuous slots or porous strips have been found to be an effective arrangement and are therefore used in various applications, for instance, in combustion chambers, afterburner nozzles, and rockets. In other applications, such as gas turbine blade cooling however, stress or manufacturing considerations make it impractical to use continuous slots or porous strips and rows of openings are preferable. A study of film cooling with such arrangements is made difficult by the three-dimensional nature of the flow and temperature fields downstream from the openings, and only sparse information is available from which the performance of this cooling method could be predicted.

The flow field, following injection from a single hole into a main stream, has received some attention. Keffer and Baines (13) and Gordier (14) reported flow visualization studies. Jordinson (15), Abramovich (16), Keffer and Baines (13), and Gordier (14) provide detailed information on pressure contours and on the location of the center line of spreading jets. All of these investigations were carried out with the secondary gas injected normal to the mainstream and with a mass velocity ratio or blowing parameter M defined by

$$M = \frac{\rho_2 U_2}{\rho_\infty U_\infty} \qquad (1)$$

greater than 2. The surface pressure distributions induced on a flat plate downstream of injection have been studied by Vogler (17). These data are obtained for injection normal to the mainstream and for a blowing parameter range from 0.2 to 1.

The qualitative descriptions of the interaction between the secondary gas and the mainstream given by Abramovich (16) and Keffer and Baines (13) are used to design the qualitative flow diagram presented in Figure 1 for a secondary flow entering through a circular tube at an angle of 35^{o} to the mainstream. As the jet of fluid leaves the hole, it retards the main flow along the upstream side of the jet causing an increased pressure there, whereas rarefaction occurs at the downstream side. This pressure difference provides the force which deflects and deforms the jet. Circulatory motions indicated in Figure 1 are caused by the intensive intermixing of the two flows. The deformation of the jet is strongly affected by the blowing rate parameter. In general, one expects that the injected fluid penetrates farther into the stream when the blowing parameter is larger. No suitable analysis is available at present which would describe quantitatively the interaction and mixing of a three-dimensional jet with a deflecting flow. Analyses presented in references (16) and (18) use models based on ideal fluids and potential

flow theory. These analyses will therefore describe actual conditions only within a few diameters distance from the point of injection.

A series of studies of the penetration of heated air jets into deflecting air streams was conducted by the NACA with secondary air introduced at a temperature approximately 160°C higher than that of the mainstream. The depth of penetration of the jet issuing from a thin plate orifice in a direction perpendicular to the deflecting flow was determined with a temperature probe (19, 20, 21). Further studies of the depth of penetration used circular, square, and elliptical orifices (20) and (21). Temperature profiles were measured for injection at angles of 90°, 60°, 45°, and 30° to the main flow direction (22, 23). The tunnel used for these experiments was quite narrow and most of the data were taken at downstream positions where the jet has already expanded to the side walls. This confinement of the jet may strongly effect the shape of the measured profiles and of the penetration depth. The studies mentioned in this paragraph appear to be the only ones which deal with the interaction of a heated jet with a deflecting flow.

The present paper reports some results of an extended investigation into film cooling with ejection of the secondary gas through a row of openings. The first phase of this study deals with ejection through a single circular hole. In a second phase, the interaction of the jets coming from neighboring

holes is being investigated. A third phase will be concerned with holes of various shapes. The aim of the entire project is to obtain a better understanding of the basic processes involved in film cooling and with this an ability to predict film cooling performance. The present report describes the adiabatic wall temperature distributions downstream of a heated jet of air issuing into a mainstream of air. The boundary layer along the wall from which the jet issues is turbulent. The secondary air enters through a long circular hole, the exit of which is made flush with the film cooled wall. The purpose of the long injection tube is to have well-defined conditions at the exit of the tube. Flow measurements are reported for injection perpendicular to the free stream and for injection through a tube inclined at an angle of 35^{o} to the mainstream. The wind tunnel used in these investigations has been designed specifically to optimize the accuracy of the investigation. The test section has been made wide enough to allow the natural spreading of the jet and sufficiently high for an unimpeded penetration of the jet injected from an injection tube with 2.5 cm diameter and directed perpendicular to the mainstream at a blowing rate parameter of approximately 2.5. In the investigation itself, the blowing parameter was varied from 0.1 to 2.

III. EXPERIMENTAL APPARATUS

A. Wind Tunnel

The wind tunnel used in this study is shown in Figure 2. The mainstream of air is drawn from the room. It passes through the entrance section, the test section, and the diffuser. From there the air is then received by a blower and discharged through a silencer to the outside. The tunnel was designed with great care and a somewhat detailed discussion may therefore be of interest.

A subsonic wind tunnel is generally designed to provide adequate flow quality in the test section with minimum power requirements. The flow quality, which is of primary concern, involves the uniformity of the velocity field, the turbulence level, flow steadiness, and absence of swirl. These factors are largely controlled by the entrance section which for the tunnel used in this investigation consists of an elliptical inlet, filter, straightening section, turbulence reducing screens, and contraction section. Since the dimensions of the other components of the entrance section depend on the dimensions of the contraction section, it is discussed first.

The area ratio of a contraction section is generally a compromise between the allowable physical size and the desirability of having a larger contraction to reduce turbulence and to obtain a uniform velocity field entering the

test section. An area ratio of 9:1 is considered adequate. A test section 20.3 cm x 20.3 cm in cross section thus results in an upstream side of the contraction 60.9 cm x 60.9 cm. The contraction length is 75 cm. Again this is a compromise between short sections which have undesirable pressure variations along their boundary and long contractions, which result in thick boundary layers at the exit. The shape of the contraction was determined by the method of Rouse and Hassan (24), which uses two cubic equations to define the upstream portion and the downstream portion of the contour.

Directly upstream of the contraction section are three screens to reduce the turbulence level. In the downstream direction these are 24 mesh[1], 40 mesh, and 60 mesh respectively, all of about 50 - 55 percent porosity (open area). The screens are placed approximately ten centimeters apart (more than 300 wire diameters) in order that the wakes from the wires be dissipated before the air enters the following screen. The upstream flow straighteners are plastic straws approximately 0.7 cm ID and 22 cm long located 15 cm upstream of the first screen. A blanket type fiberglass filter is placed directly ahead of the straighteners to eliminate dust from the incoming air.

---

[1]The mesh size indicates the number of wires per inch (i.e. 2.54 cm)

The inlet portion to the entrance section has the same shape as an inviscid jet issuing from an infinitely large container through a 79 cm x 79 cm square aperture. In this way the pressure along the inlet wall is constant, thus avoiding flow separation and minimizing the boundary layer thickness. The values for the profile were obtained from Reference (24) and approximated by a quarter ellipse.

The diffuser gives a smooth, efficient transition from the 20.3 cm x 20.3 cm test section to the 51 cm diameter blower inlet. It has an equivalent total opening angle of 8.4 degrees. Flow straighteners, to prevent blower swirl from feeding back into the test section, are located downstream of the diverging section. These straighteners are made of tubes 3.8 cm diameter by 30 cm long which are enclosed in a cylindrical housing. A flow control unit is attached to the downstream side of the flow straightener housing. It has the form of a circular cylinder with sixteen 2.54 cm and eight 7.6 cm diameter holes located in two rows around its periphery. Sliding bands with corresponding holes are located around the cylinder such that the effective hole opening can be varied. In this way an adjustable part of the flow through the blower can be made to bypass the tunnel. The coarse adjustment is also made by means of a radial inlet damper on the blower.

B. Secondary Flow System

The secondary or injected air is supplied by the compressor of the laboratory. After being filtered it passes through a pressure regulator which reduces the pressure and eliminates pressure fluctuations. Following the regulator is a needle valve which controls the air flow rate.

Temperature fluctuations introduced by the compressor are eliminated by passing the air through 30 meters of 2.54 cm diameter coiled copper tubing which is submerged in a large tank of water. This gives a stable temperature condition at the inlet of the heater used to raise the injection air temperature. Before entering the heater the flow rate of the secondary air is measured with a thin plate orifice meter.

The orifice assembly is designed in accordance with the ASME Power Test Code (25). Four orifice plates were used to cover the range of flow rates and their coefficients were determined by calibration with water measuring the flow rate by weighing. The results of the calibration are in excellent agreement with the tabulated values for sharp edged orifices presented in Reference (25) having a maximum deviation of less than 0.5%.

In the wind tunnel assembly, the secondary air passes from the orifice assembly to the heater which consists

of a stainless steel tube, 2.3 cm ID x 3.2 meters long, wrapped with three heating tapes (each capable of producing 768 watts,) and insulated. The heaters are wired such that one of them can be operated at either zero or full power, one can be operated at zero, half, or full power and one can be operated over a continuous range from zero to full power. Thus, any heat input between 0 and 2304 watts can be obtained. The heated air passes to the plenum chamber of the injection section which is discussed in the next section.

C. Test Section

The test section of the wind tunnel has an overall length of 129.8 cm or 153.8 cm depending upon the injection configuration. The side walls and top are constructed of plexiglas and the bottom wall of Textolite.

The test section is composed of three segments. The first segment is 20.3 cm long and attached rigidly to the end of the contraction section. Its bottom wall is thin (0.32 cm thick) in order to allow it to respond rapidly to any changes in the temperature of the main flow. A 0.064 cm diameter boundary layer trip wire is located on the bottom wall of this segment approximately 3.8 cm downstream from the end of the contraction section.

Proceeding in the flow direction, the next segment is the injection section. In this section the secondary air is introduced into the tunnel. The length of this segment is 6.5 cm

for normal injection and 30.5 cm for injection at an angle of 35^{o} to the main flow. The bottom wall of this segment is made of 0.64 cm thick Textolite.

The secondary gas is injected through a 2.35 cm ID stainless steel tube approximately one meter long, glued into the bottom plate of the injection segment, and ground flush to the tunnel surface. The tube length guarantees the establishment of a well defined velocity profile at the point of injection. In order to reduce heat conduction from the tube the bottom wall of the section is thinned from the back side to a thickness of 0.32 cm in the region surrounding the injection tube. Thermocouples are soldered on the outside of the tube at distances of one half, four and one half, and six diameters from the discharge end and the tube is surrounded by insulation. At the upstream end of the injection tube is located a plenum chamber approximately 7.5 cm in diameter and 10 cm long containing a series of baffles and screens which act to eliminate any nonuniformity of velocity or temperature introduced by the heat exchanger. A sharp edged entrance is used between the plenum chamber and tube to accelerate the flow development in the tube. The bottom wall of the injection segment is connected to the test section in a manner which allows it, together with the tube and plenum chamber, to slide in a direction normal to the tunnel axis. The injection of the secondary gas can thus be located at any lateral position in the tunnel which permits

the use of a single row of thermocouples to measure lateral wall temperature distributions downstream of the injection.

The third segment of the test section is 103 cm long and is fastened rigidly to the diffuser. Its bottom wall is an adiabatic test plate as indicated in Figure 3 designed according to the following considerations: it should have a rapid thermal response and it should be adiabatic, this means the plate should not only be well insulated in a direction normal to its surface, it must also have negligible conduction in all directions parallel to the surface, since local adiabatic temperature measurements are desired. The design chosen is shown in Figure 3. It consists of a thin Textolite plate 0.32 cm thick backed by approximately 5 cm of Styrofoam insulation. The thin plate is supported at each edge by a rigid member running the full length of the section and in the interior by a series of 0.48 cm diameter Textolite pins spaced as shown in Figure 3. The height of these pins is adjustable to allow the elimination of low or high spots in the plate surface.

Three rows of calibrated 36 gauge iron-constantin thermocouples are installed in the adiabatic test plate. Forty-five are located along the axis of the section and eleven at a distance 7.5 cm on either side of the axis. Two methods of installation are used as shown in the lower part of Figure 3. The plate is relieved on the back side to a thickness of 0.16 cm in the region surrounding each junction in order to reduce

conduction through the plate. The test section is also equipped with static pressure taps on the bottom and side walls.

Since the adiabatic wall is thin, the static pressure difference between the inside and outside of the tunnel produced by the mainstream flow is sufficient to deform the plate between its supports. Therefore, a cover is used to seal the region below the insulated test plate. The space between the back of the test plate and the cover is held at a pressure equal to the static pressure inside the tunnel by means of two tubes leading from this space to the diffuser section at a position immediately downstream of the test section.

D. Instrumentation

The boundary-layer velocity profiles are obtained by measuring the total pressure with a small flattened total pressure probe and the static pressure with taps located on the side wall of the tunnel. The tip of the total pressure probe is made from 0.091 cm OD stainless steel hypodermic tubing, the end of which is thinned to 0.0038 cm wall thickness, then flattened to a 0.0076 cm opening and honed smooth. The probe is mounted on a sliding carriage which has a micrometer head. The assembly provides both vertical and axial positioning of the probe tip. The probe can be inserted through one of three grooves cut in the top of the tunnel test section at positions on the axis of the tunnel and 6.5 cm to either side of the axis. The

measurements off the tunnel axis check the lateral uniformity of the main flow.

Velocity and temperature profiles of the secondary fluid as it enters the test section were measured with no main flow. A total pressure probe, the tip of which is made from 0.127 cm OD x 0.022 cm wall thickness stainless steel hypodermic tubing and a 36 gauge iron-constantan thermocouple mounted on a traversing assembly driven by a micrometer head were used for this purpose. The static pressure was taken as the ambient pressure surrounding the jet. The thermocouple was attached such that the junction extends approximately 0.3 cm beyond the velocity probe tip.

To measure the free stream velocity for normal operating conditions of the tunnel, either of the two total pressure probes is used in conjunction with a side wall static pressure tap.

IV. TUNNEL OPERATING CONDITIONS

In order to define the operating conditions in the tunnel, velocity profiles in the boundary layer on the bottom wall of the test section, as well as velocity and temperature profiles of the secondary flow at the exit of the injection tube are presented.

The wall boundary layer profiles were taken at various axial positions with no secondary injection. Velocity profiles, obtained in the absence of a trip, indicate that the naturally developing boundary layer in the region of injection is neither

laminar nor fully turbulent. Therefore, a 0.064 cm diameter trip wire was located on the bottom wall of the test section approximately 3.8 cm downstream from the end of the contraction section. With the trip wire a fully developed turbulent velocity profile was found to exist on the test surface. At any axial position in the tunnel, the velocity profiles at the center line and those 6.5 cm on either side of the center line are in agreement indicating the uniformity of flow across the tunnel.

The profiles were taken with the tunnel assembled with either injection segment and at mainstream velocities of 30.5 and 61.0 meters per second. The end of the injection tube was sealed and moved to lateral position away from the line along which the profiles were being taken. A representative number of the profiles taken along the centerline of the tunnel are presented in Figure 4. These dimensionless profiles are seen to be in good agreement with each other and with the profile reported by Klebanoff and Diehl (26).

Under the assumption that the boundary layer originates as a turbulent one, it is possible to determine from the velocity measurements the effective starting position of the boundary layer and with it to define flow conditions in the test section. If the shear stress at the wall is expressed by the Blasius relation

$$\tau_w \propto \rho_\infty U_\infty^2 \left(\frac{\nu_\infty}{U_\infty \delta}\right)^{1/4} \tag{2}$$

the boundary-layer growth can be expressed in terms of the displacement thickness

$$\delta^* = C\ (\nu_\infty/U_\infty)^{1/5}\ (X)^{4/5} \tag{3}$$

where the displacement thickness, δ^*, is defined as

$$\delta^* = \int_0^\infty \left[1 - \frac{\rho U}{\rho_\infty U_\infty}\right] dY \tag{4}$$

The value δ^* can be determined by integration of the measured velocity profiles. Since equation (3) shows that $(\delta^*)^{1.25}$ is proportional to X, curves of $(\delta^*)^{1.25}$ versus the distance from the trip wire, X', can be extrapolated to the position where δ^* is zero, thereby determining the effective location of the start of the turbulent boundary layer. This procedure is used in Figure 5 for the two mainstream velocities used in the investigation. Also included in this figure are values of the momentum thickness, δ_i, obtained from

$$\delta_i = \int_0^\infty \left[1 - \frac{\rho U}{\rho_\infty U_\infty}\right] \frac{U}{U_\infty}\ dY \tag{5}$$

The axial positions at which injection occurs for the adiabatic wall temperature measurements are indicated in Figure 5.

To have reproducible inlet conditions for the secondary air the test program called for a fully developed turbulent velocity profile at the end of the injection tube in the absence of freestream flow. Velocity profiles were, therefore, taken in planes normal to the tube axis at two tube Reynolds numbers with the probe tip located just inside the tube exit. A representative velocity profile (which is essentially invarient for the two tube orientations and tube Reynolds numbers) is presented in Figure 6. It is symmetric about the centerline of the tube and agrees well with the results of Nikuradse, (27), for fully developed turbulent flow in smooth pipes. Temperature profiles were obtained for the 35^{o} injection configuration at essentially the same location as for the velocity profiles. A representative profile is also presented in Figure 6. It is symmetric and quite flat.

V. ADIABATIC WALL TEMPERATURES

Previous studies on film cooling with a continuous slot established the fact that heat transfer coefficients can be calculated with relations for convective heat transfer without ejection of a secondary fluid, provided the heat transfer coefficients are defined with the adiabatic wall temperature (2).

This procedure has not yet been checked for film cooling with injection through holes. It was felt, however, that the information most urgently needed is the adiabatic wall temperature. The present section presents adiabatic wall temperature distributions downstream of a heated jet of air issuing into a mainstream. Data were obtained with injection through a tube inclined at an angle of 35^{o} to the mainstream and through a tube perpendicular to the mainstream. The secondary air was introduced into the tunnel at a temperature approximately $55^{o}C$ above that of the mainstream. After waiting and checking for thermal equilibrium, the wall temperatures, mainstream temperature and injection gas temperature were measured. The adiabatic wall temperatures are reported in the form of a film cooling effectiveness:

$$\eta = \frac{T_{aw} - T_{\infty}}{T_2 - T_{\infty}} \tag{6}$$

The adiabatic wall temperature, T_{aw}, is measured by the thermocouples installed along the centerline of the test plate. By moving the injection section laterally, this row of thermocouples can be used to measure the axial temperature distribution at various lateral positions, Z, relative to the jet. The mainstream temperature, T_{∞}, is measured in two ways, by means of

thermocouples located in the mainstream flow upstream of the injection position and by thermocouples in the test plate at positions unaffected by the injection. These two measurements are in agreement. The secondary air temperature, T_2, is taken as that measured by the thermocouples attached to the injection tube at positions 4½ and 6 diameters upstream of its end (both of which indicate the same temperature). These locations are far enough upstream from the tube exit to be insensitive to temperature distortions caused by the mainstream flow any by the conduction from the tube to the injection plate. Figure 6 shows the effect of this heat conduction in the absence of a main flow. The values of the injection temperature, T_2, and bulk temperature, T_{Bulk}, are also indicated. It should be noted that although the bulk temperature is probably the most representative injection temperature it is very difficult to measure the velocity and temperature profiles necessary to calculate it in the presence of primary flow. Figure 6 shows that T_2 gives a good representation of the temperature of the secondary flow. Special tests were also performed to determine the error that conduction from the injection region introduces in the wall temperature readings. The injection tube was heated to normal operating temperatures (i.e. approximately 55^{o}C above mainstream) without mass injection and wall temperature measurements were taken at two mainstream velocities (~30 m/sec and 61 m/sec). The effect of conduction was found to be negligible.

Film cooling effectiveness distributions are presented for different values of the blowing rate parameter in Figures 7 through 16. The data presented in these figures are for an injection angle of 35^{o}. Two mainstream velocities (represented in dimensionless form as $U_{\infty}D/\nu_{\infty}$) are considered. For the purpose of discussion first consider the results of the tests performed at $U_{\infty}D/\nu_{\infty} = 0.87 \times 10^{5}$. In Figure 7 (M = 0.1), the film cooling effectiveness decreases with increasing axial distance for lateral positions on or near the centerline of the jet. This decrease is reminiscent of the results obtained with a continuous slot. At sufficiently large Z/D, however, the effectiveness is seen to increase rather than decrease with increasing axial distance. These positions are beyond the edge of the injection tube. At small values of X/D the jet has not spread to these lateral positions. As the jet progresses downstream it spreads laterally thereby accounting for the increase in effectiveness.

At larger values of the blowing rate parameter, M = 0.2 (Figure 8) and M = 0.5 (Figure 9) the same trends are observed. In going from M = 0.1 to M = 0.5 the overall level of effectiveness is increased. This agrees with results for film cooling with injection through a continuous slot where, for this range of blowing rates, increased mass injection leads to higher effectiveness. In the two-dimensional case Wieghardt (1) finds that, except close to the injection slot, the film cooling

effectiveness is well represented by the relation

$$\eta = 21.8 \left(\frac{X}{MS} \right)^{-0.8} \tag{7}$$

where S is the slot height. The value MS is the injected mass flow rate per unit span of the system divided by the mainstream mass flow rate per unit area. For a row of holes it is possible to find an effective slot height which is the total area for mass injection divided by the span. This effective slot height is dependent on the center spacing of the injection holes and (as used in Eq. (7) and on Figure 9) would be π times the tube diameter divided by four times the spacing between holes expressed in tube diameters. Two reference curves are presented in Figure 9 in which the film cooling effectiveness is calculated using Eq. (7) and the effective slot heights, S, for 2-diameter and 3-diameter center to center tube spacing. The reference lines are presented on this figure because in the present investigation the maximum film cooling effectiveness is obtained for $M \cong 0.5$. The difference in the present results from the film cooling observed using two-dimensional slots can be attributed to the penetration of the jet flow into the mainstream and the subsequent flow of mainstream air down between the jet and the wall.

At still higher values of the blowing rate parameter, presented in Figure 10 (M = 0.75) and Figure 11 (M = 1.0) the

level of the film cooling effectiveness decreases with increasing blowing rate. This is contrary to what occurs with film cooling using a continuous slot and is apparently due to the increased penetration of the secondary flow into the primary stream at large values of M. Figures 12 through 16 exhibit the same trends for the case of $U_\infty D/\nu_\infty = 0.44 \times 10^5$. At the highest blowing rate studied (Fig. 16) the film cooling effectiveness near the point of injection first increases with distance downstream, apparently due to the increased jet penetration. In an effort to qualitatively see what is happening at the high injection rates, small tufts of thread attached to a wire were placed in the flow field. By this means it was observed that the jet penetrates some distance into the mainstream. The "void" on the downstream side of the jet caused by the penetration is filled by air from the mainstream. As the tuft is moved farther downstream the jet is turned into the direction of the main flow losing its velocity component normal to the wall simultaneously spreading such that it then touches the bottom wall. This penetration followed by reattachment through spreading could account for the increasing cooling effectiveness downstream of the injection point for large blowing rate parameters.

A cross plot of the data for an injection angle of 35^o is presented in Figure 17 where the film cooling effectiveness at a number of axial positions is presented as a function of the blowing rate parameter. At any axial position the effectiveness

first increases as the injection rate is increased, reaches a maximum, and then decreases with increased injection. The maximum occurs at $M \cong 0.5$. With film cooling through a continuous slot similar trends have been observed with a maximum being reached for $M \cong 1$.

The lateral film cooling effectiveness distributions at a number of axial positions are shown for two values of the blowing rate parameter in Figure 18. The shape of these curves resembles the velocity and temperature distributions in a free jet (16). Close to the injection location (small X/D) the effectiveness decreases rapidly as one proceeds laterally from the centerline of the jet. An important feature in this figure is the relatively small amount of spreading. Observe that if one were to use a single row of holes in an effort to film cool a surface, the center to center spacing of the holes would have to be quite small unless conduction in the wall equalized the temperatures. If, for example, the holes are located 3 diameters apart, the position midway between the holes occurs at Z/D = 1.5, a position at which little or no cooling would be achieved. The spreading of the jet is also indicated in Figure 26 which will be discussed later.

Examination of the data for injection normal to the main flow presented in Figures 19 through 25 reveals trends which are similar to those encountered for 35 degree injection. The film cooling effectiveness decreases with increasing axial distance

for lateral positions on or near the centerline of the jet. At sufficiently large Z/D, the effectiveness first increases with increasing axial distance and then decreases.

One significant trend differs in the results for the two injection configurations. As mentioned previously, with large blowing rates (M = 1.5 and 2.0) at an angle of 35 degrees the increased jet penetration causes the wall temperature to first increase and then decrease with increasing axial distance for all lateral positions. This does not occur with normal injection as shown in Figure 25. Instead, the same basic shape of the axial effectiveness distributions is observed for all injection rates, possibly due to the increased mixing which occurs when the injection is normal to the mainstream.

The effect of injection angle has been considered in a study sponsored by General Electric Company. The coolant was injected through a row of holes inclined at either 15^{o} or 35^{o} to the main flow. Near the holes the film cooling effectiveness with the 15^{o} inclination does not fall off rapidly with blowing rate while it does with the 35^{o} injection holes. Farther downstream the variation with injection rate for both configurations has a dependence on blowing rate similar to that encountered using continuous slots.

The spreading of both the 35^{o} and 90^{o} jets is indicated in Figure 26 where the parameter $Z_{\frac{1}{2}}/D$ is presented as a function of axial distance downstream of the injection location, X/D. The value $Z_{\frac{1}{2}}$ is defined as the lateral position at which the film cooling effectiveness is equal to one-half its value at

Z of zero. Figure 26 consists of two graphs with injection angles of 90^{o} and 35^{o} respectively with each graph containing curves for values of the blowing rate parameter from 0.1 to 2.0. In general the spreading of the jet is greater for the case of perpendicular injection probably due to the more intensive interaction which occurs when the streams are directed normal to each other.

It is interesting to note that the spreading of the jet with normal injection is almost the same as that for 35^{o} injection at very low blowing rates. With a small amount of secondary gas addition the temperature field probably comes close to that generated by a point heat source located in the surface at the position of the holes. This analogy may open the way to an analytical prediction of film cooling effectiveness.

The effect of the blowing rate, M, on the spreading of the jet is also shown in Figure 27 where the parameter $Z_{\frac{1}{2}}/D$ is presented as a function of the blowing rate for both 90^{o} and 35^{o} injection at one particular axial location ($X/D \cong 30$). With injection at an angle of 35^{o} the spreading decreases with increasing injection rate according to Figure 27 until a value of $M = 0.75$ is attained. Beyond this value, the spreading is approximately independent of M. For perpendicular injection, on the other hand, the trend is reversed for $M \leq 1$; as the blowing rate parameter increases the spreading increases. If the blowing rate parameter is increased beyond $M = 1$ the spreading decreases.

For comparison, the thermal spreading of a heated circular jet, coaxial to a main flow, is also presented in Figure 26 for the two values of the blowing rate parameter $M = \infty$ (i.e. $U_{\infty} = 0$)

and M = 2.0. These lines are determined from information presented by Abramovich (16). From his figures it can be determined that the temperature spread is approximately 1.4 times greater than the velocity spread and that the position at which the velocity difference is one-half the difference between the jet centerline velocity and the mainstream velocity is approximately 0.46 times the distance between the centerline and edge of the jet. Applying these factors to the information presented in (16) for the lateral spreading of the total width of a jet as a function of the downstream distance from the plane of efflux of the jet, it is possible to approximate the thermal spreading.

A comparison of the effectiveness in the axial direction for the two injection angles at the same mainstream velocity and injection rate reveals that higher effectiveness is usually obtained for 35^{o} injection. This result is consistent with the point previously discussed that greater spreading exists for the case of normal injection. The more intensive interaction which occurs when the secondary flow is perpendicular to the main flow tends not only to spread the jet but also to lower its temperature.

Figure 28 shows the effect of the Reynolds number $U_{\infty}D/\nu_{\infty}$ of the mainstream on the film cooling effectiveness. The figure presents information specifically for the case of M = 0.5 and Z/D = 0 for an angle of injection of 35^{o}. It is seen that an increase in the Reynolds number produces a slight rise in the effectiveness. A possible explanation for this is that the dimensionless boundary layer thickness δ^*/X' decreases with increasing $U_{\infty}D/\nu_{\infty}$. For example, at the upstream edge of the

issuing jet $\delta^* = 0.135$ cm for $U_\infty D/\nu_\infty = 0.44 \times 10^5$ while at the same position $\delta^* = 0.12$ cm for $U_\infty D/\nu_\infty = 0.87 \times 10^5$. As the injected air enters the mainstream boundary layer it encounters a higher relative velocity at positions close to the wall for the thinner boundary layer. This would have the effect of turning the injected air more rapidly, decreasing its penetration and therefore leading to slightly higher values of the film cooling effectiveness.

VI. RESUMÉ

An experimental investigation has been conducted to determine the adiabatic wall temperature distribution with film cooling on a flat plate. An air stream flows along the flat surface forming a turbulent boundary layer and secondary air is injected into this stream from a circular tube which ends flush with the surface. Two tube orientations are used: one in which the tube axis is normal to the adiabatic wall and one in which the tube axis is inclined at an angle of 35° to the wall. The adiabatic wall temperature is defined as that temperature which is established in steady state at any location on the surface under the influence of the flow described above when heat conduction within the plate and radiative transfer are absent.

Basic trends for the two injection angles were found to be similar with differences occurring only at large injection

rates. Sizeable differences in the level of cooling, however, were found to exist between the two angles of injection. Injection at an angle of 35^{o} to the mainstream was found to yield higher cooling effectiveness than that with 90^{o} injection.

The film cooling effectiveness for both injection angles was found to be considerably different from that obtained when secondary fluid is introduced through a continuous slot.

The film cooling effectiveness for injection through discrete hole was found to reach a maximum for mass flow ratios (ratios of the product of density and velocity of the secondary air to mainstream air) of about 0.5.

The spreading of the secondary air jet was small. These results indicate that injection with a single row of holes located as close as three diameters apart would provide little or no cooling at locations midway between the holes.

At low values of mass flow ratios, injection at either 35^{o} or 90^{o} to the mainstream creates approximately the same spreading angle for the adiabatic wall temperature fields. The spreading angle increases at air injection angles of 90^{o} with mass flow ratios up to 1 and then decreases. At an injection angle of 35^{o}, the spreading angle decreases with mass flow ratios up to 0.75 and then stays approximately constant.

Increasing the mainstream Reynolds number (decreasing the ratio of the mainstream boundary layer thickness to tube diameter) results in a slight increase in the film cooling effectiveness.

ACKNOWLEDGMENTS

The authors wish to express their appreciation to R. R. Brannon, D. R. Pedersen, T. C. Nelson and F. J. Patoile for their aid in obtaining and reducing the experimental data.

REFERENCES

(1) K. Wieghardt, "Hot-Air Discharge for De-icing," AAF Translation, Report No. F-TS-919-Re, Wright Field (1946).

(2) J. P. Hartnett, R. C. Birkebak and E. R. G. Eckert, "Velocity Distributions, Temperature Distributions, Effectiveness and Heat Transfer for Air Injected Through a Tangential Slot into a Turbulent Boundary Layer," J. Heat Transfer, Trans. ASME Series C. 83, 293-306 (1961).

(3) E. R. G. Eckert and R. C. Birkebak, "The Effects of Slot Geometry on Film Cooling," Heat Transfer, Thermodynamics and Education, ed. H. A. Johnson, McGraw-Hill Book Co. Inc., 150-163 (1964).

(4) R. A. Seban, "Heat Transfer & Effectiveness for Turbulent Boundary Layer with Tangential Fluid Injection," J. Heat Transfer, Trans. ASME Series C, 82, 303-312 (1960).

(5) S. Papell and A. M. Trout, "Experimental Investigation of Air Film Cooling Applied to an Adiabatic Wall by Means of an Axially Discharging Slot," NASA TN D-9 (1959).

(6) R. J. Goldstein, G. Shavit and T. S. Chen, "Film Cooling Effectiveness with Injection Through a Porous Section," J. Heat Transfer, Trans. ASME Series C. 87, 353-361 (1965).

(7) N. Nishiwaki, M. Hirata and A. Tsuchida, "Heat Transfer on a Surface Covered by Cold Air Film," International Developments in Heat Transfer, ASME, New York, 675-681 (1961).

(8) R. J. Goldstein, R. B. Rask and E. R. G. Eckert, "Film Cooling With Helium Injection into an Incompressible Air Flow," Int. J. Heat Mass Transfer, 9, 1341-1350 (1966).

(9) M. Tribus and J. Klein, "Forced Convection from Nonisothermal Surfaces," Heat Transfer Symposium, University of Michigan Press, Ann Arbor, Michigan, 211-235 (1953).

(10) J. Librizzi and R. J. Cresci, "Transpiration Cooling of a Turbulent Boundary Layer in an Axisymmetric Nozzle," AIAA Journal, 2, 617-624 (1964).

(11) S. S. Kutateladze and A. I. Leont'ev, "Film Cooling with a Turbulent Gaseous Boundary Layer," Thermal Phys. High Temp., 1, 281-290 (1963).

(12) R. J. Goldstein and A. Haji-Sheikh, "Prediction of Film Cooling Effectiveness," Paper No. 225, JSME Semi-International Symposium (1967).

(13) J. F. Keffer and W. D. Baines, "The Round Turbulent Jet in a Cross Wind," J. Fluid Mech., 15, 4, 481-497 (1963).

(14) R. L. Gordier, "Studies on Fluid Jets Discharging Normally into Moving Liquid," St. Anthony Falls Hyd. Lab., University of Minnesota, Tech. Paper, No. 28, Series B. (1959).

(15) R. Jordinson, "Flow in a Jet Directed Normal to the Wind," Aero. Res. Council, R & M, No. 3074 (1956).

(16) G. N. Abramovich, The Theory of Turbulent Jets, M.I.T. Press, Massachusetts Institute of Technology, Cambridge, Massachusetts, 3-25, 195-201, 541-556 (1963).

(17) R. D. Vogler, "Surface Pressure Distributions Induced on a Flat Plate by a Cold Air Jet Issuing Perpendicularly from the Plate and Normal to a Low-Speed Free-Stream Flow," NASA TN D-1629 (1963).

(18) J. P. Fraser, "Three-Dimensional Study of a Jet Penetrating a Stream at Right Angles," Journal of the Aero. Sciences, 21, 1, 59-61 (1954).

(19) E. E. Callaghan and R. S. Ruggeri, "Investigation of the Penetration of an Air Jet Directed Perpendicularly to an Air Stream," NACA TN 1615 (1948).

(20) E. E. Callaghan and D. T. Bowden, "Investigation of Flow Coefficient of Circular, Square, and Elliptical Orifices at High Pressure Ratios," NACA TN 1947 (1949).

(21) R. S. Ruggeri, E. E. Callaghan and D. T. Bowden, "Penetration of Air Jets Issuing From Circular, Square, and Elliptical Orifices Directed Perpendicularly to an Air Stream," NACA TN 2019 (1950).

(22) E. E. Callaghan and R. S. Ruggeri, "A General Correlation of Temperature Profiles Downstream of a Heated-Air Jet Directed Perpendicularly to an Air Stream," NACA TN 2466 (1951).

(23) R. S. Ruggeri, "General Correlation of Temperature Profiles Downstream of a Heated Air Jet Directed at Various Angles to Air Stream," NACA TN 2855 (1952).

(24) H. Rouse and M. M. Hassan, "Cavitation-Free Inlets and Contractions," Mechanical Engineering, 71, 3, 213-216 (1949).

(25) "ASME Power Test Codes," Supplement on Instruments and Apparatus, Part 5, Chap. 4 (1959).

(26) P. S. Klebanoff and Z. W. Diehl, "Some Features of Artificially Thickened Fully Developed Turbulent Boundary Layers with Zero Pressure Gradient," NACA Report 1110 (1952).

(27) J. Nikuradse, "Gesetzmaessigkeiten der turbulenten Stroemung in glatten Rohren," VDI-Forschungsheft, 3, B, 356 (1932).

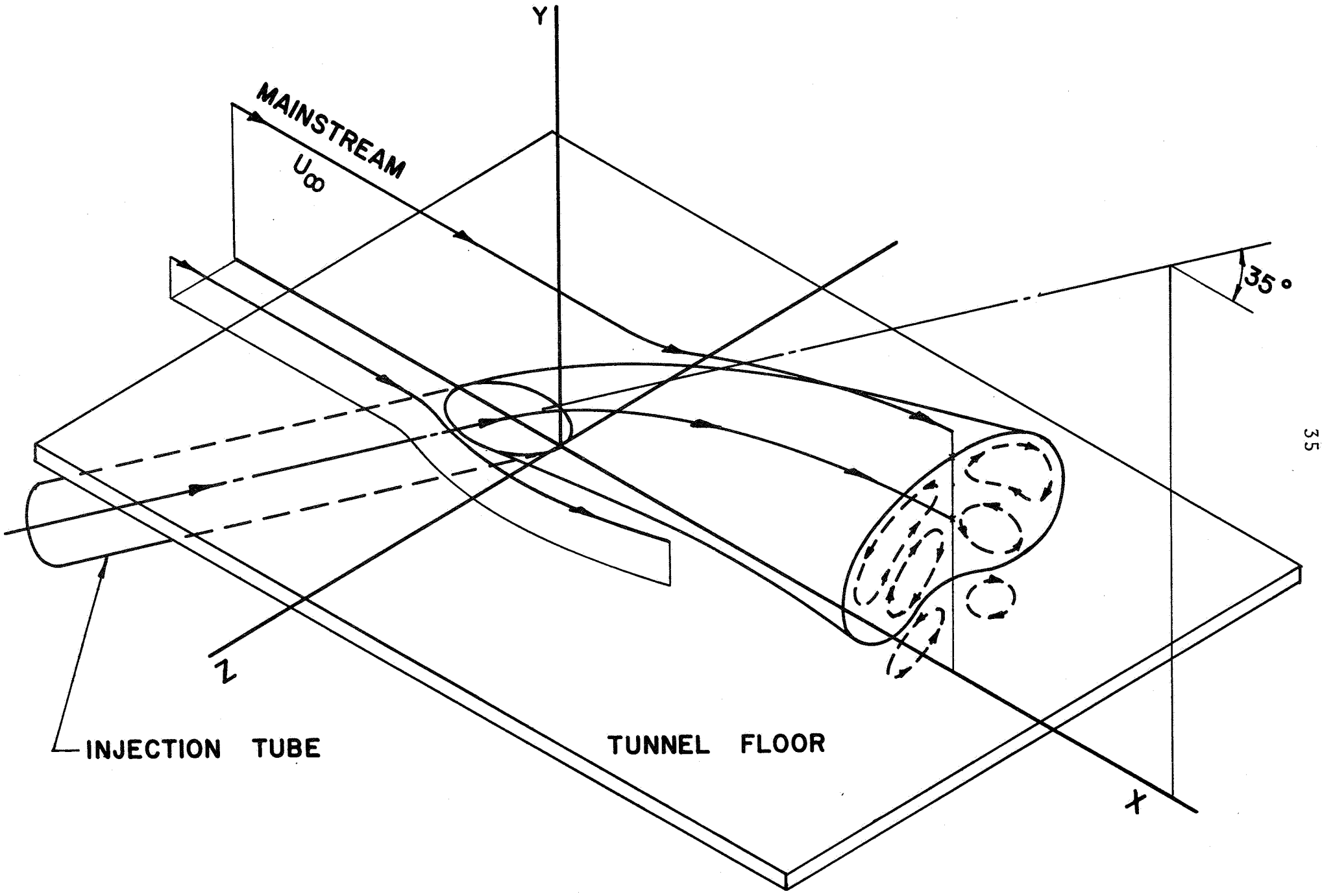
Y
MAINSTREAM
U_∞
35°
Z
INJECTION TUBE
TUNNEL FLOOR
X

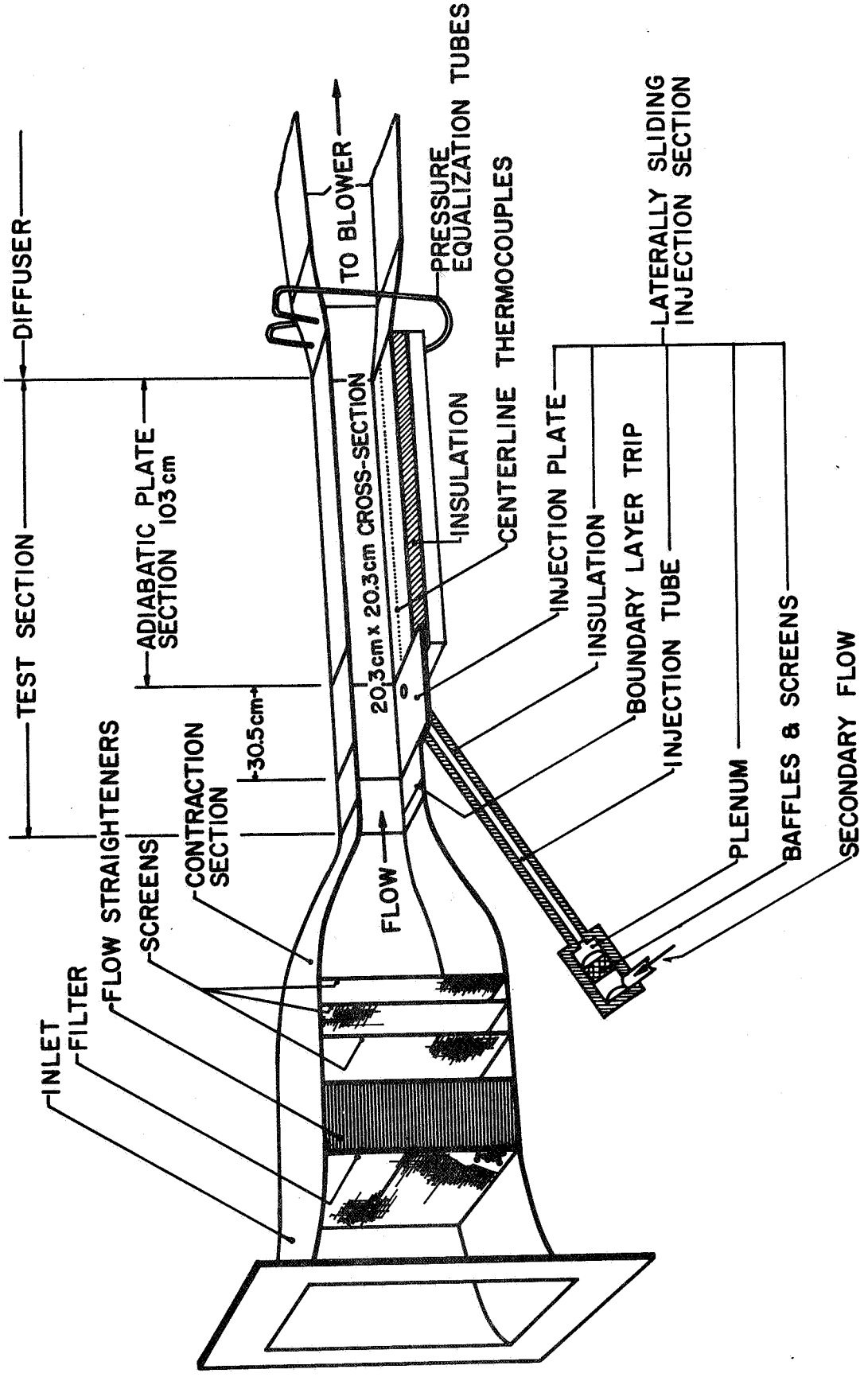

Fig. 2 Wind tunnel used in present studies

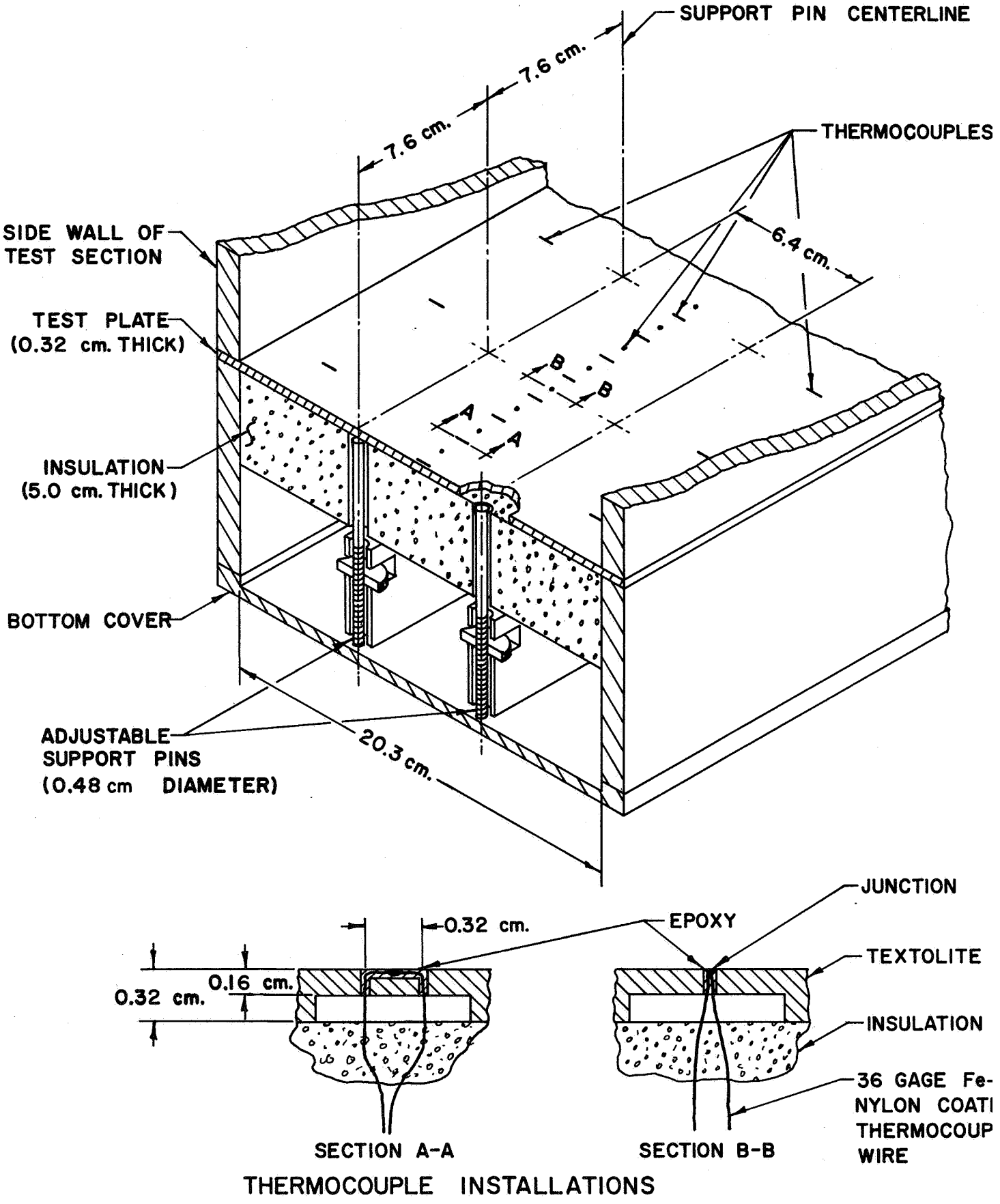

Fig. 3 Detail of adiabatic test plate and thermocouple installations

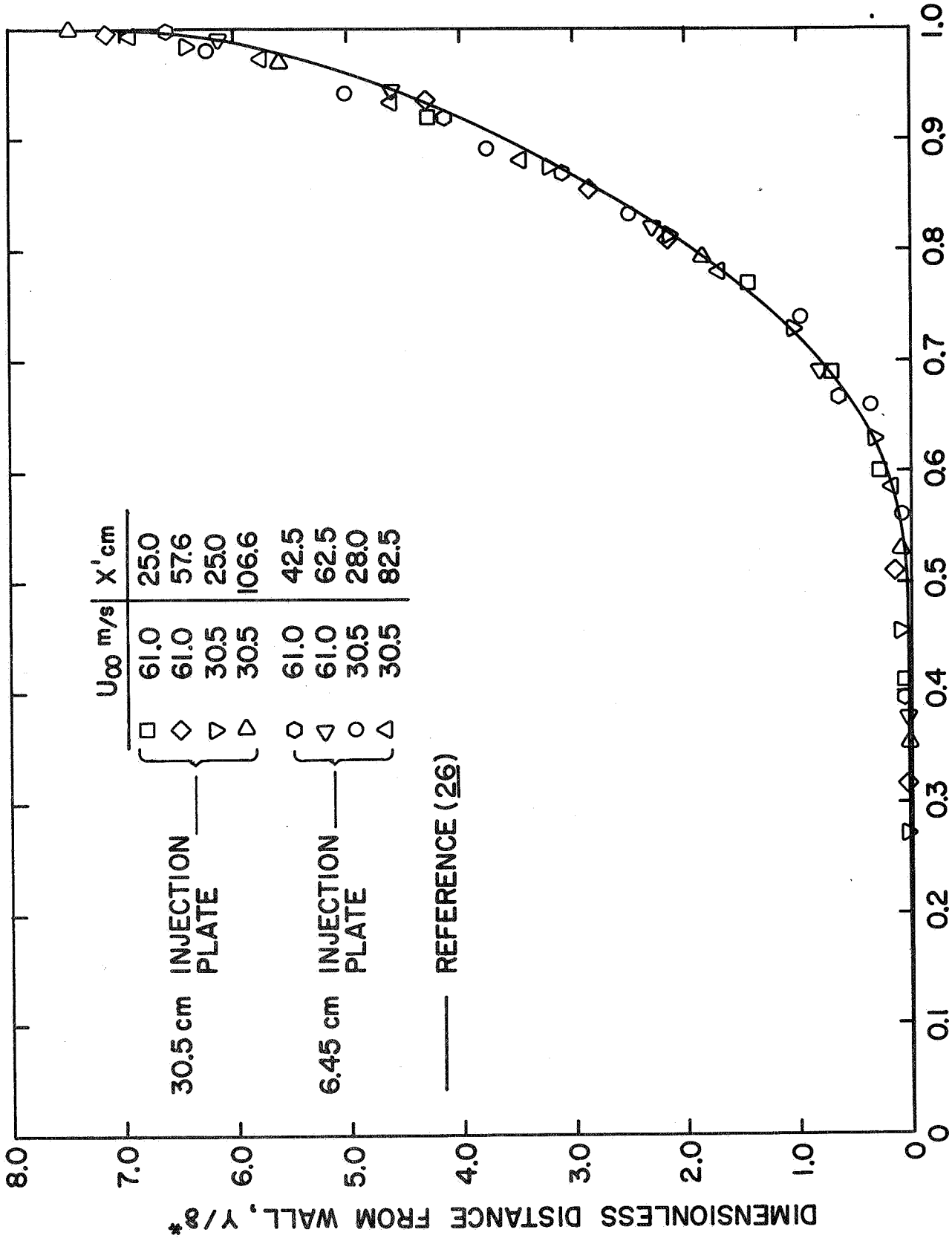

Fig. 4 Boundary layer velocity profiles along adiabatic wall with no secondary gas flow

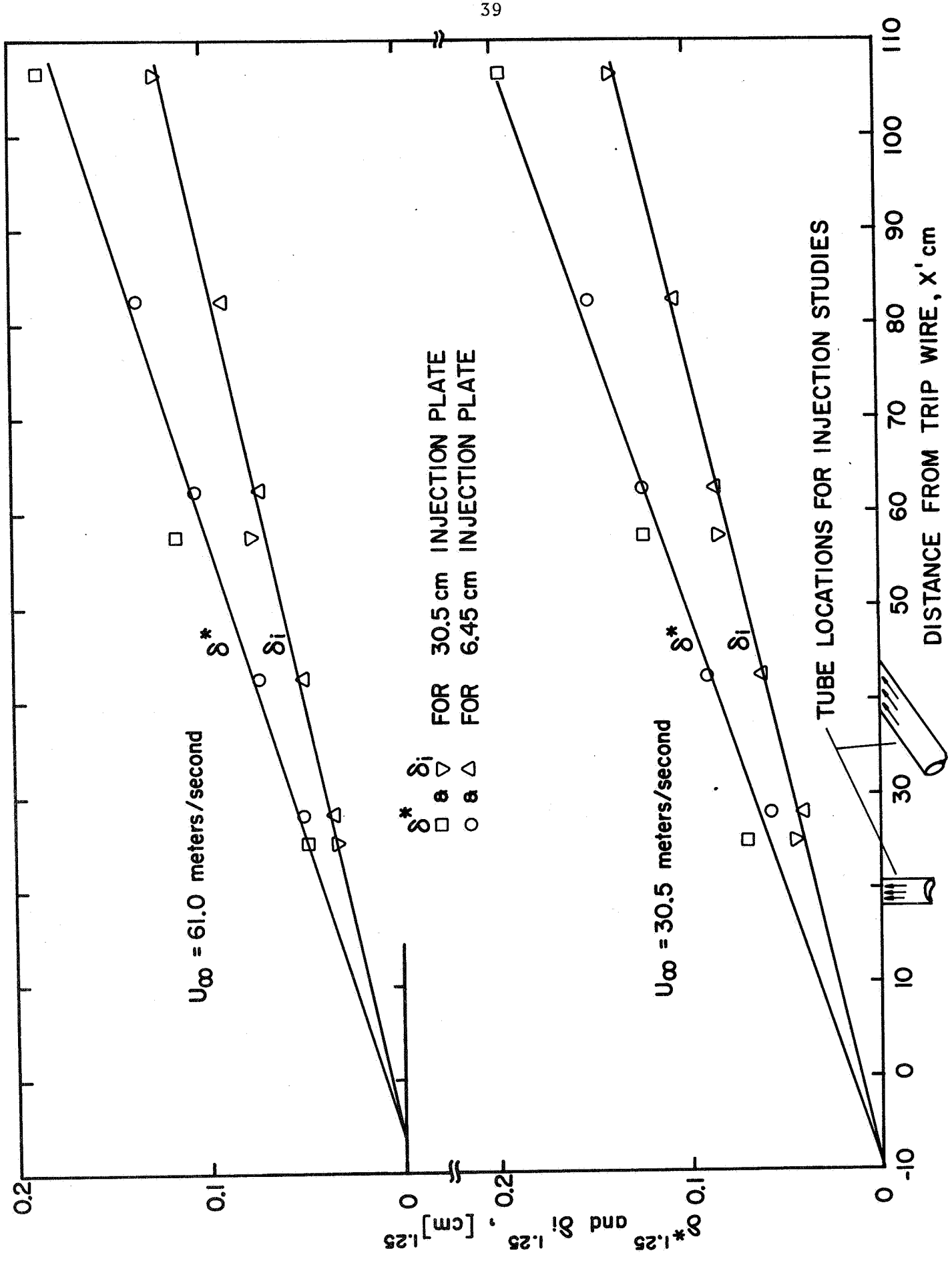

Fig. 5 Boundary layer growth

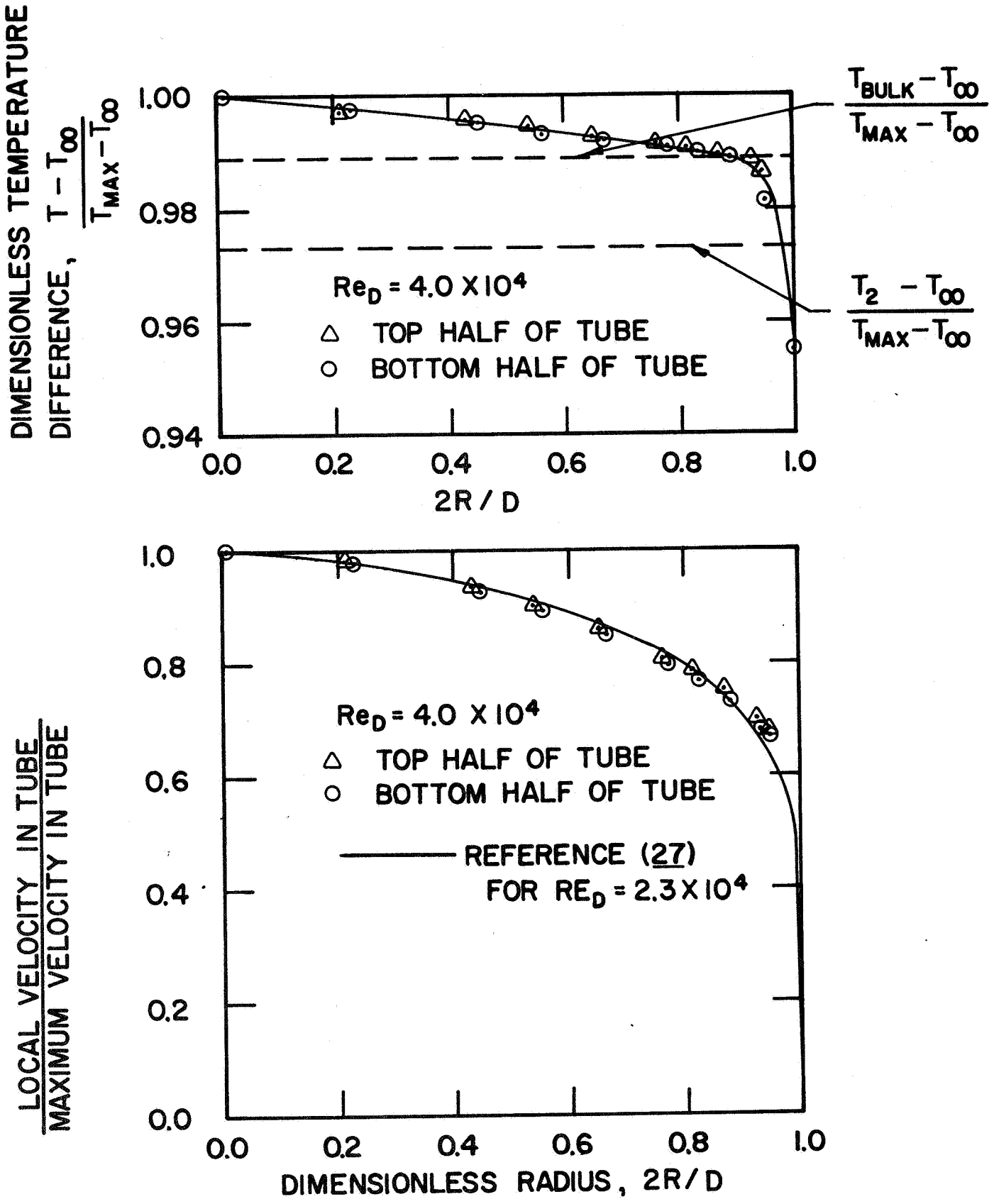

Fig. 6 Injection tube velocity and temperature profiles when no main flow is present

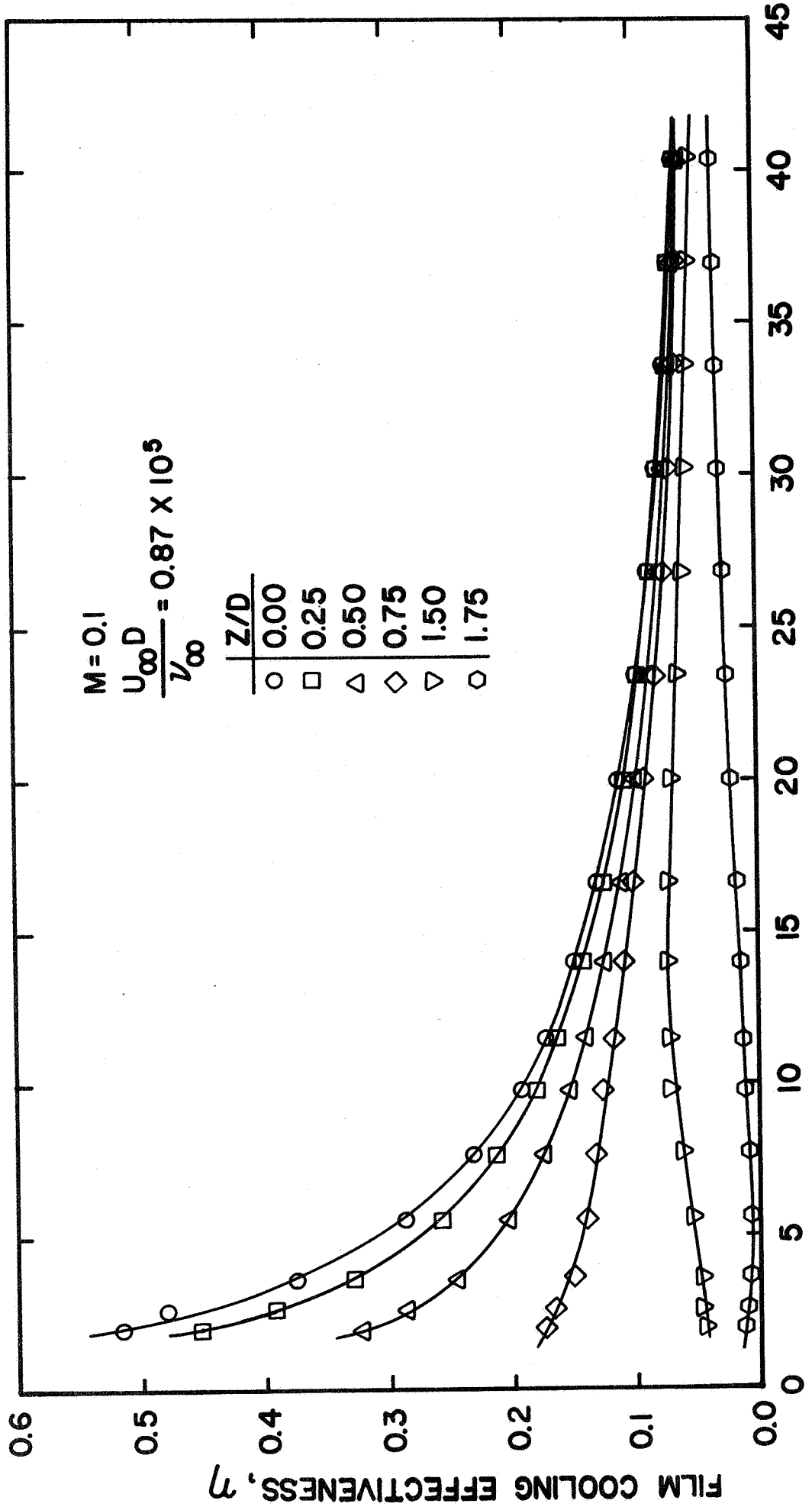

Fig. 7 Axial effectiveness distributions for 35^o injection angle, M = 0.1

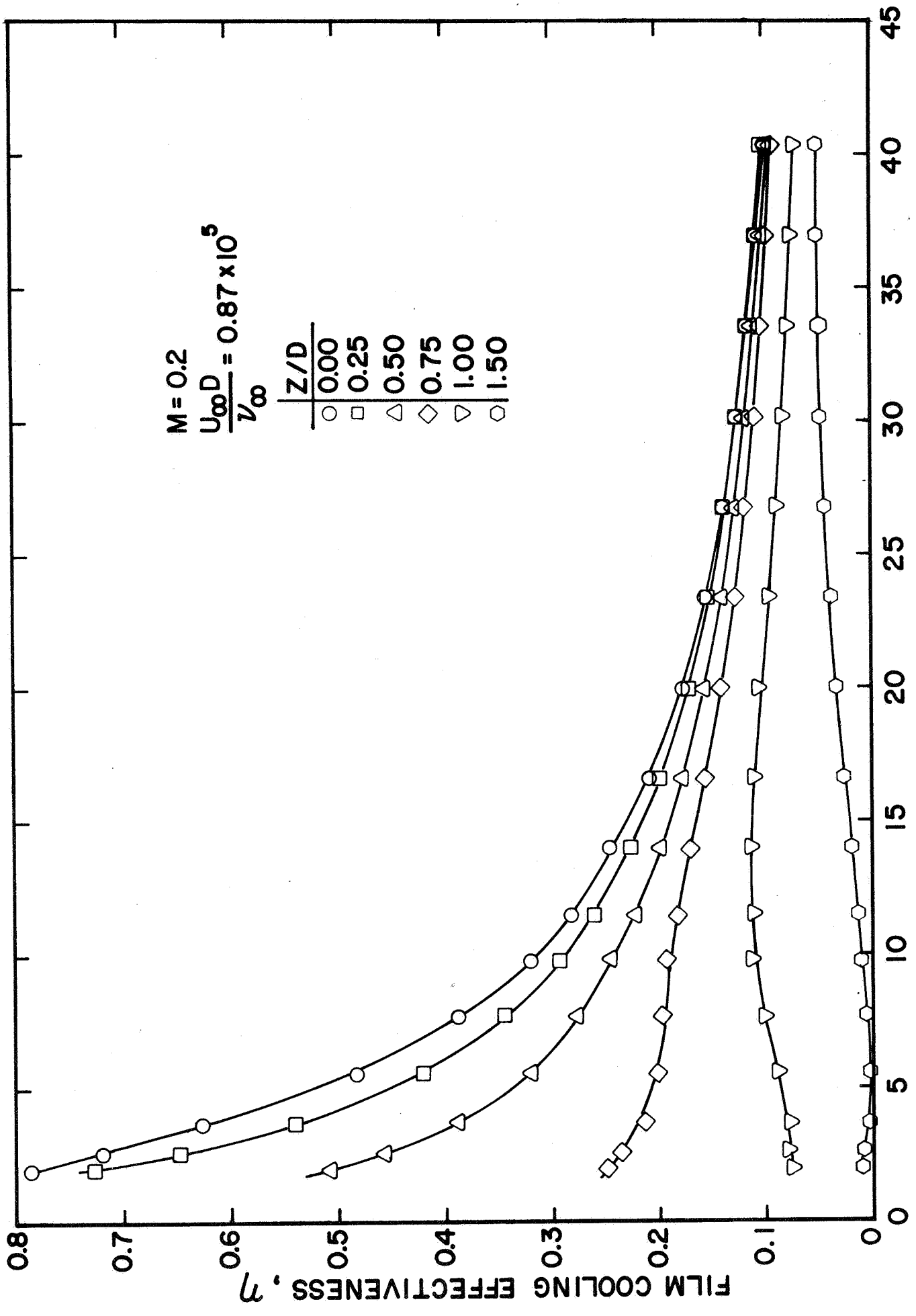

Fig. 8 Axial effectiveness distributions for zr° injection angle, M = 0.2

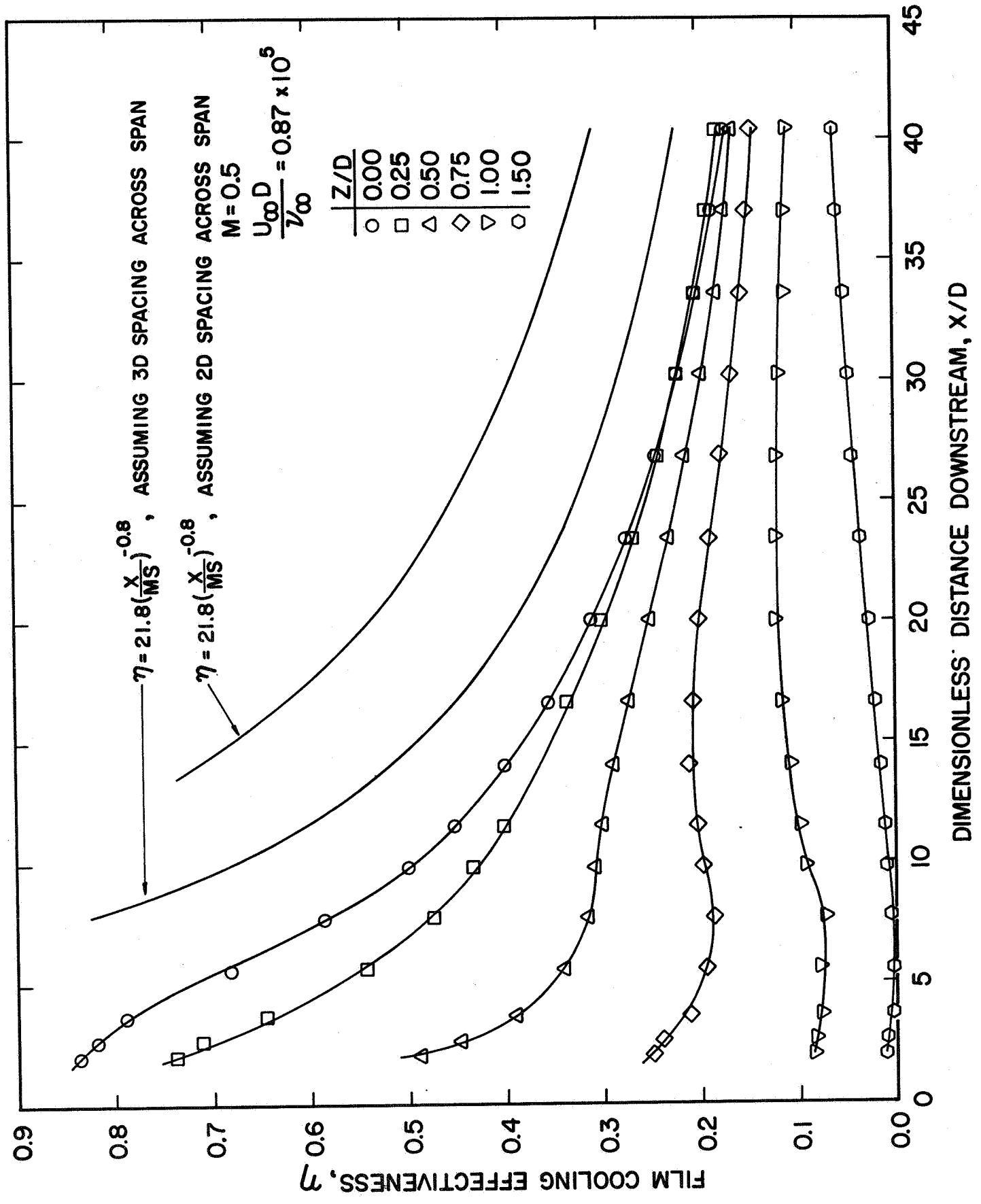
FILM COOLING EFFECTIVENESS, η
DIMENSIONLESS DISTANCE DOWNSTREAM, X/D
η = 21.8(X/MS)^-0.8, ASSUMING 3D SPACING ACROSS SPAN
η = 21.8(X/MS)^-0.8, ASSUMING 2D SPACING ACROSS SPAN
M = 0.5
U∞D/ν∞ = 0.87 x 10^5
Z/D
0.00
0.25
0.50
0.75
1.00
1.50
0.0
0.1
0.2
0.3
0.4
0.5
0.6
0.7
0.8
0.9
0
5
10
15
20
25
30
35
40
45

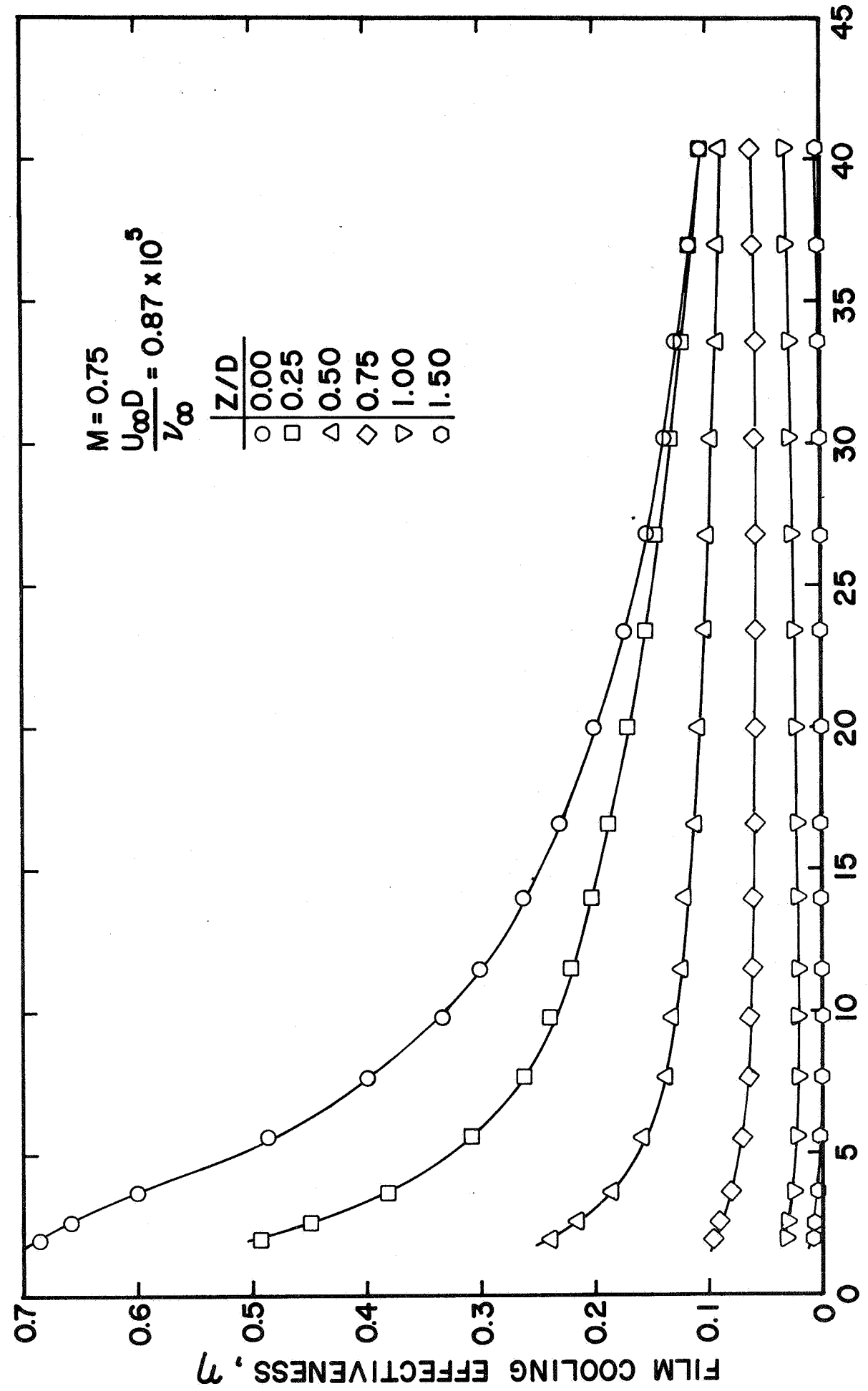
M = 0.75
$\frac{U_\infty D}{\nu_\infty} = 0.87 \times 10^5$
Z/D
0.00
0.25
0.50
0.75
1.00
1.50
FILM COOLING EFFECTIVENESS, η
0.7
0.6
0.5
0.4
0.3
0.2
0.1
0
0
5
10
15
20
25
30
35
40
45
DIMENSIONLESS DISTANCE DOWNSTREAM, X/D

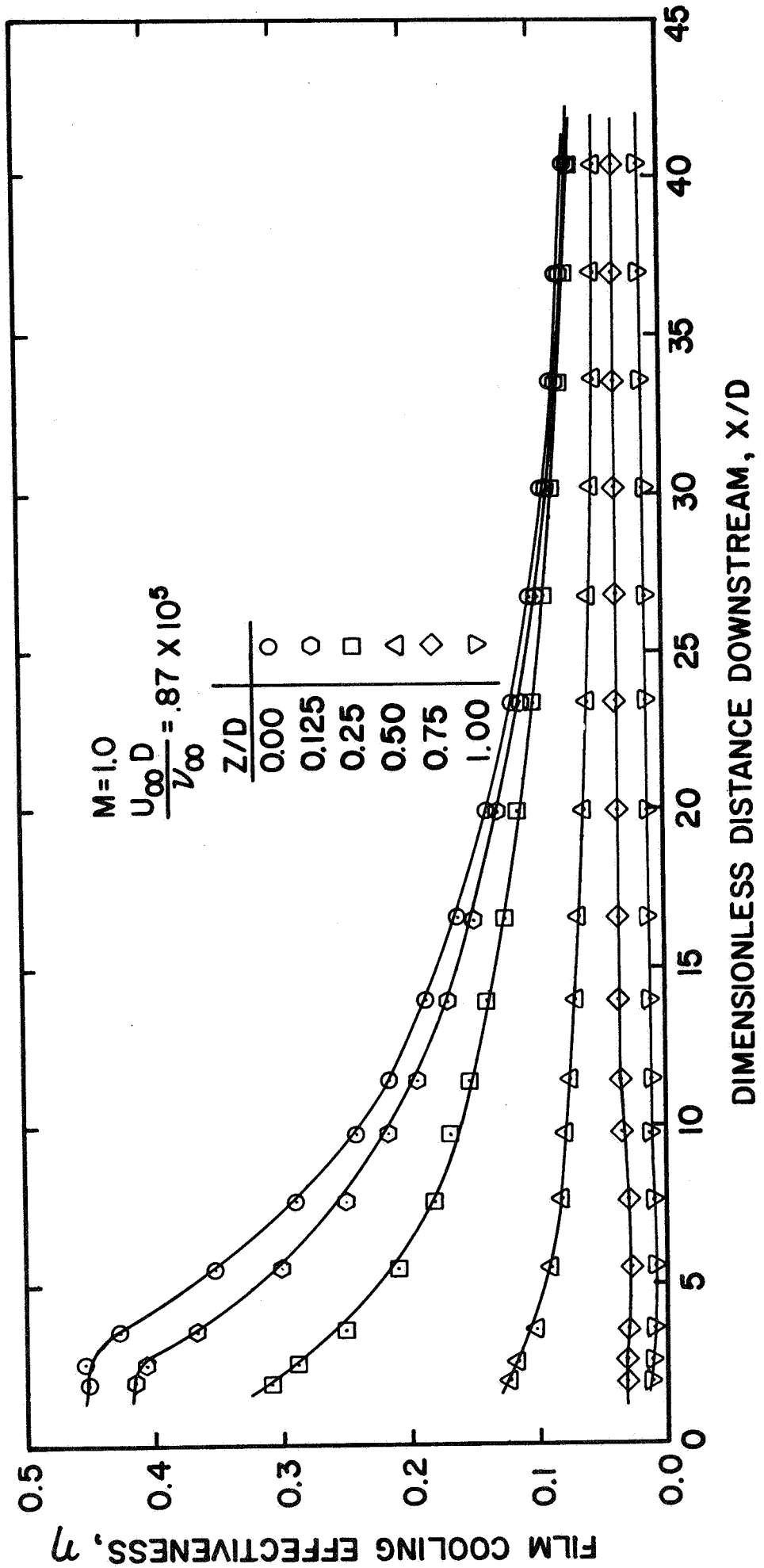

Fig. 11 Axial effectiveness distributions for 35^o injection angle, M = 1.0

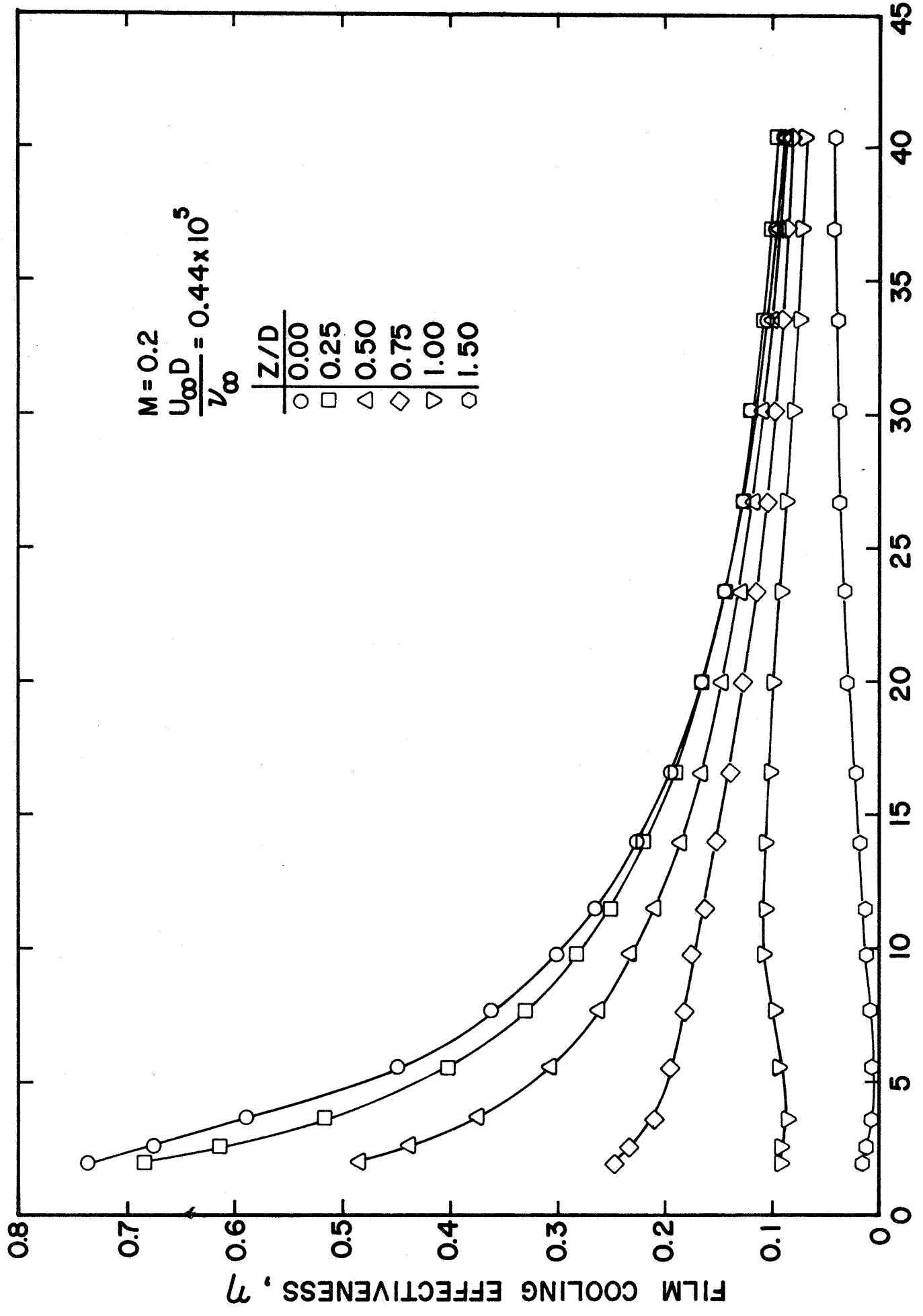

Fig. 12 Axial effectiveness distributions for 35° injection angle, M = 0.2

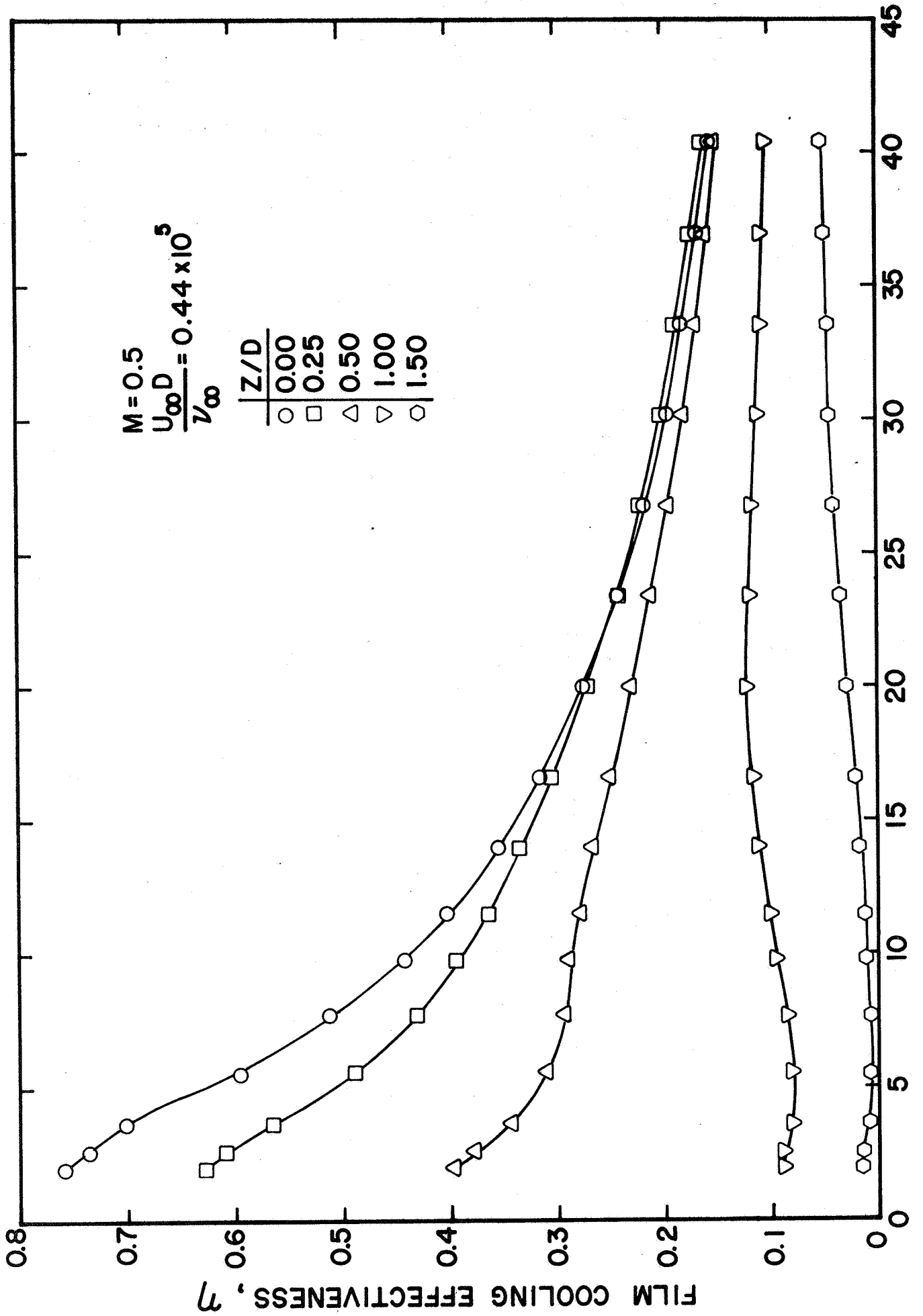
M=0.5
$\frac{U_\infty D}{\nu_\infty} = 0.44 \times 10^5$
Z/D
0.00
0.25
0.50
1.00
1.50
FILM COOLING EFFECTIVENESS, η
DIMENSIONLESS DISTANCE DOWNSTREAM, X/D
0.8
0.7
0.6
0.5
0.4
0.3
0.2
0.1
0
0
5
10
15
20
25
30
35
40
45

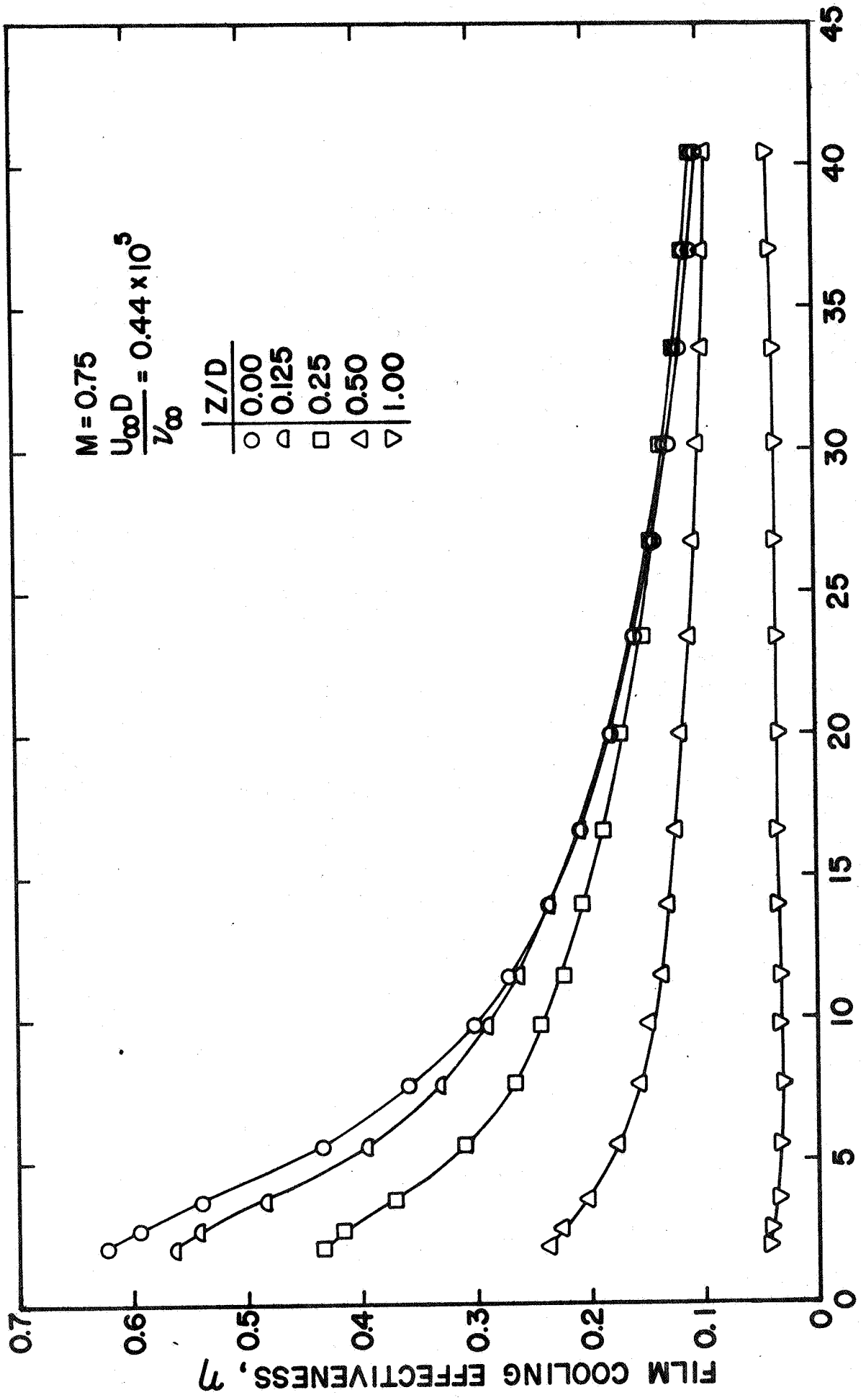

Fig. 14 Axial effectiveness distributions for 35° injection angle, M = 0.75

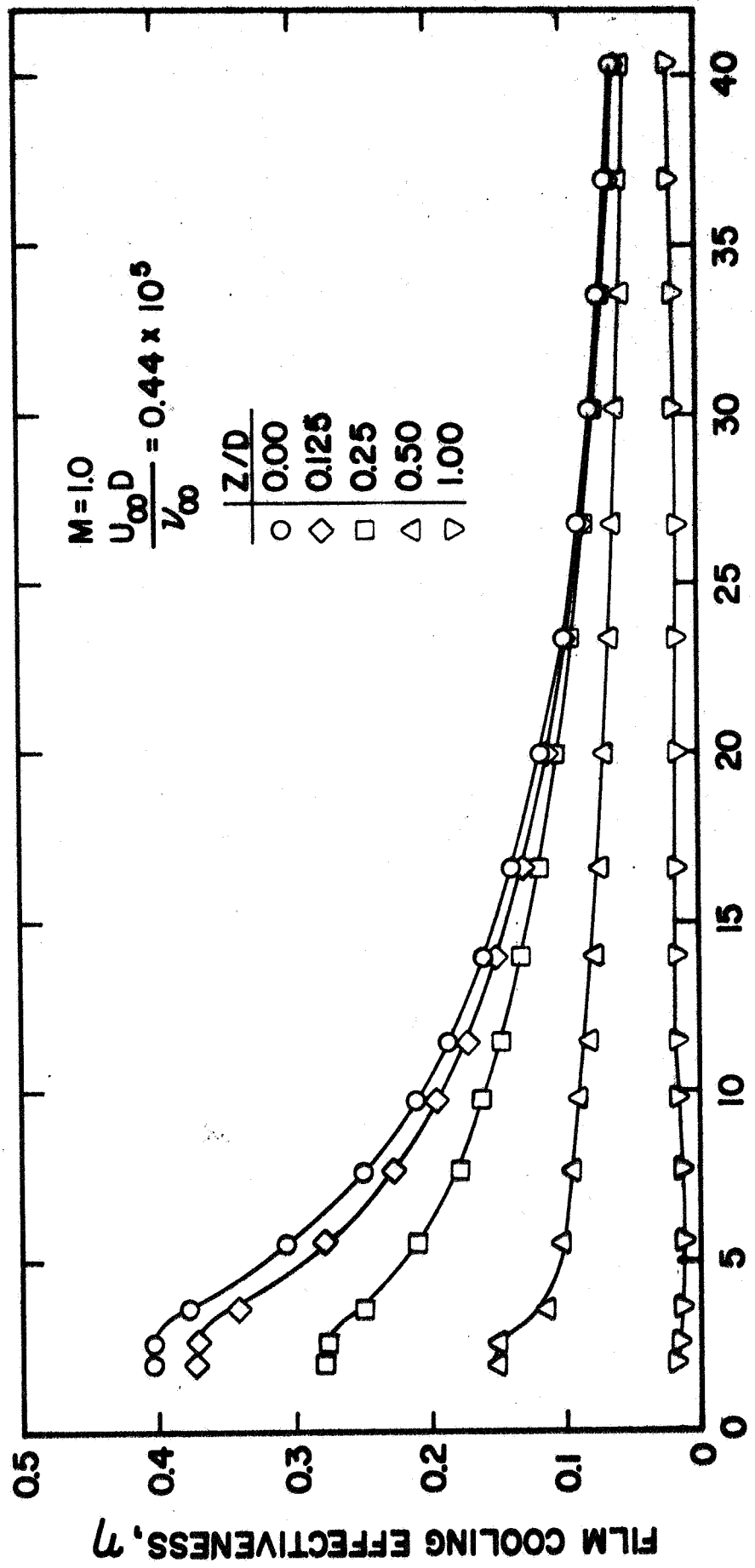

Fig. 15 Axial effectiveness distributions for 35° injection angle, M = 1.0

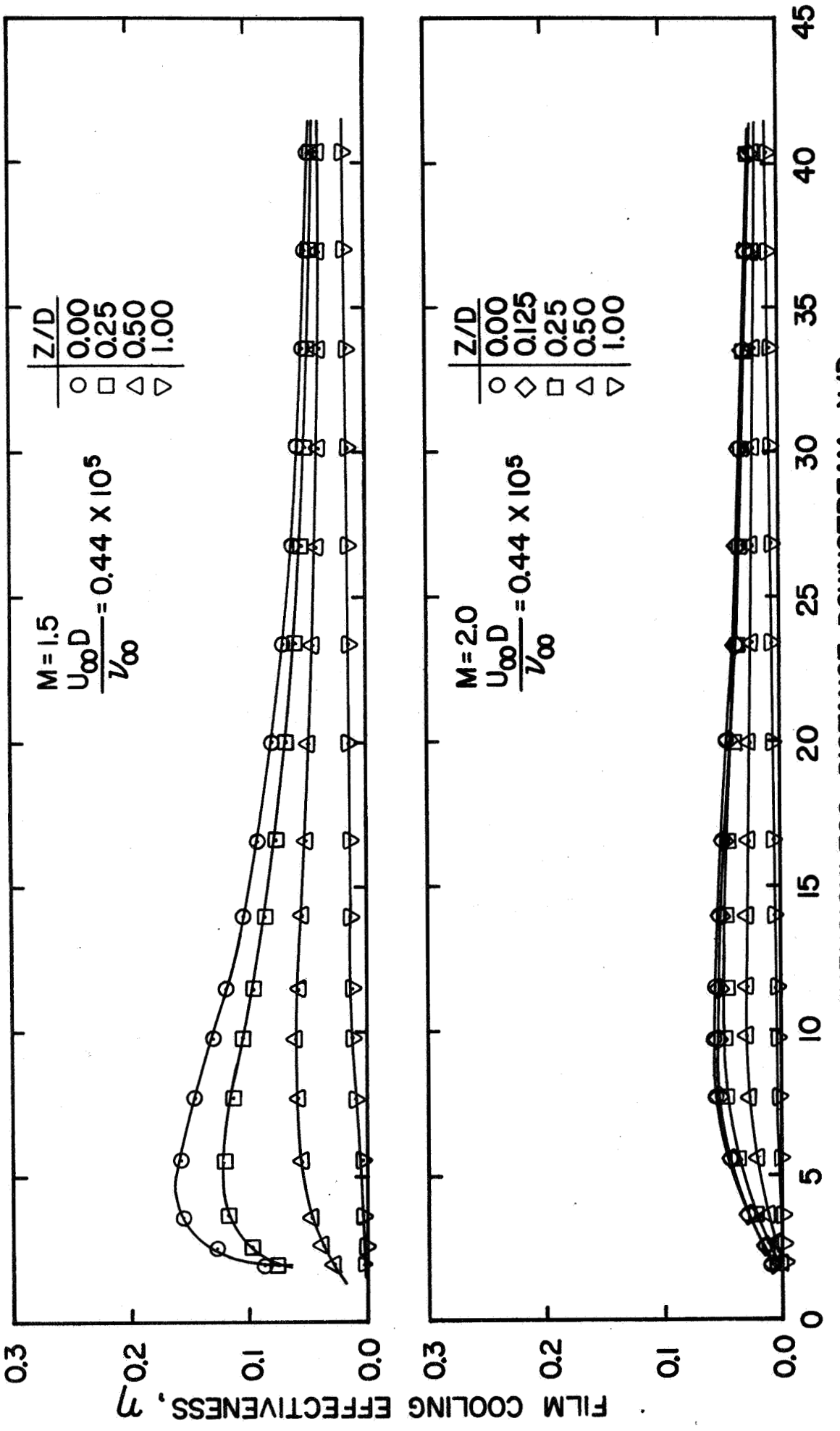

Fig. 16 Axial effectiveness distributions for 35^{o} injection angle, M = 1.5 and M = 2.0

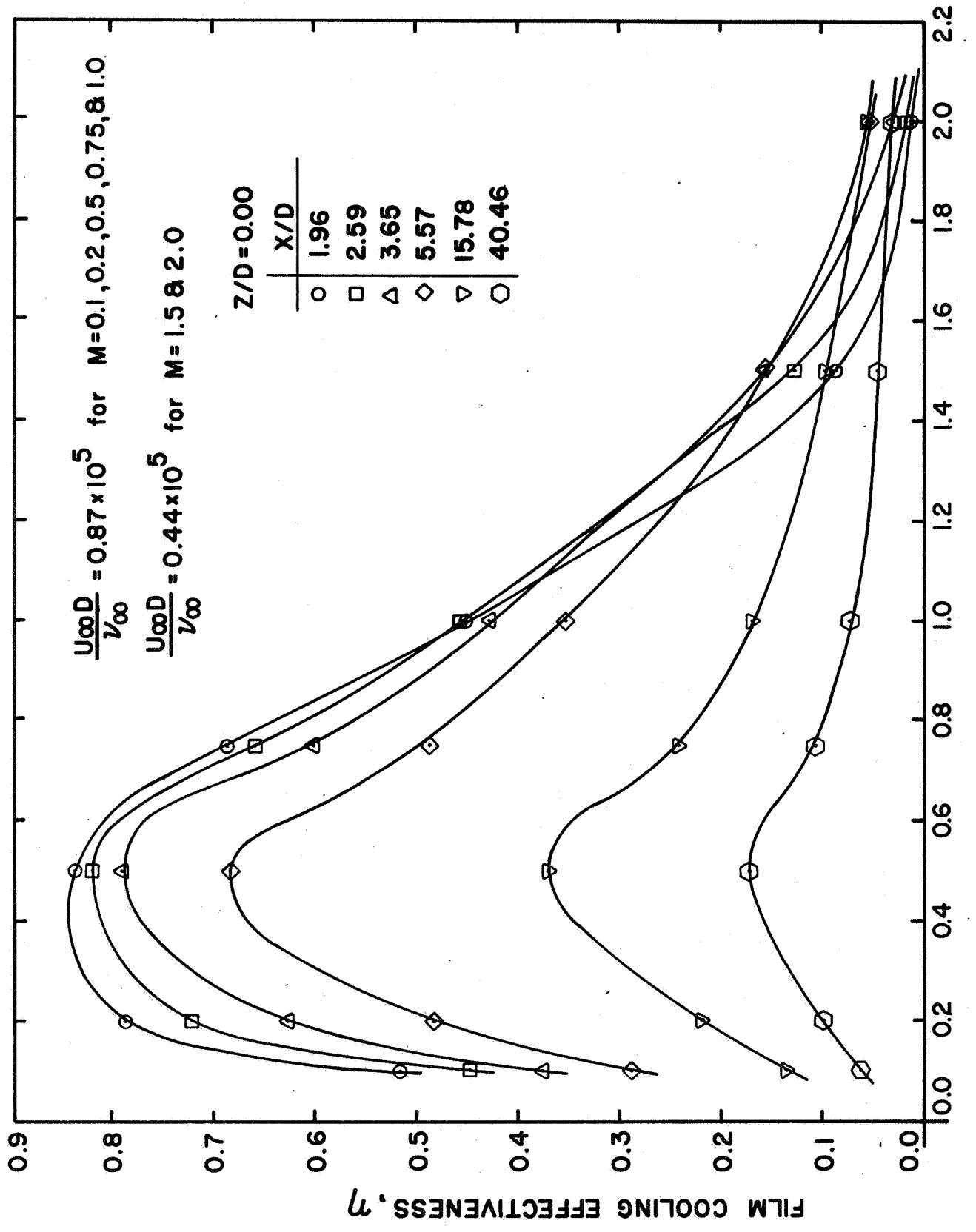

Fig. 17 Effect of blowing rate parameter on the film cooling effectiveness for injection at

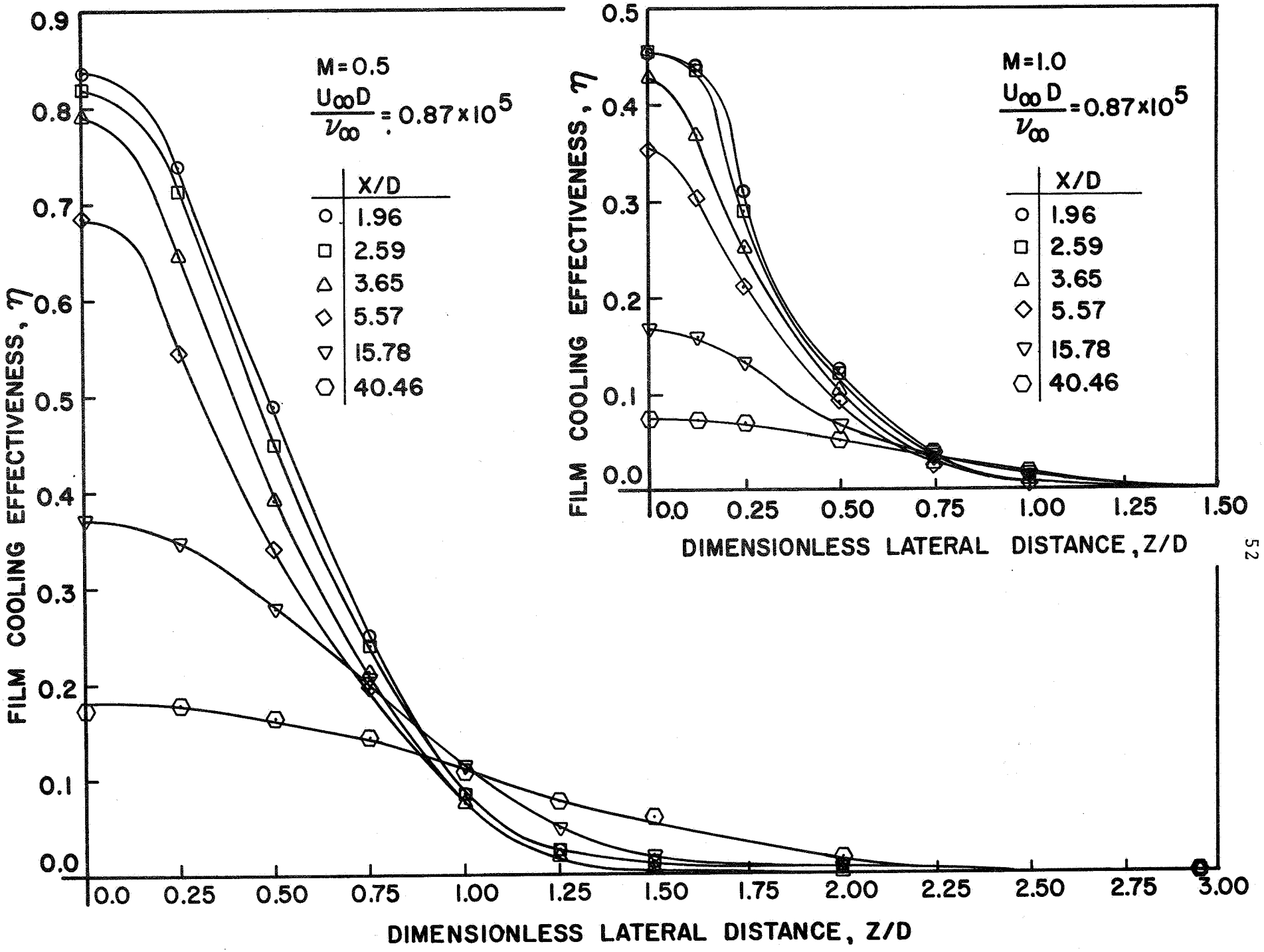

Fig. 18 Lateral effectiveness distributions for 35^o injection angle, M = 0.5 and M = 1.0

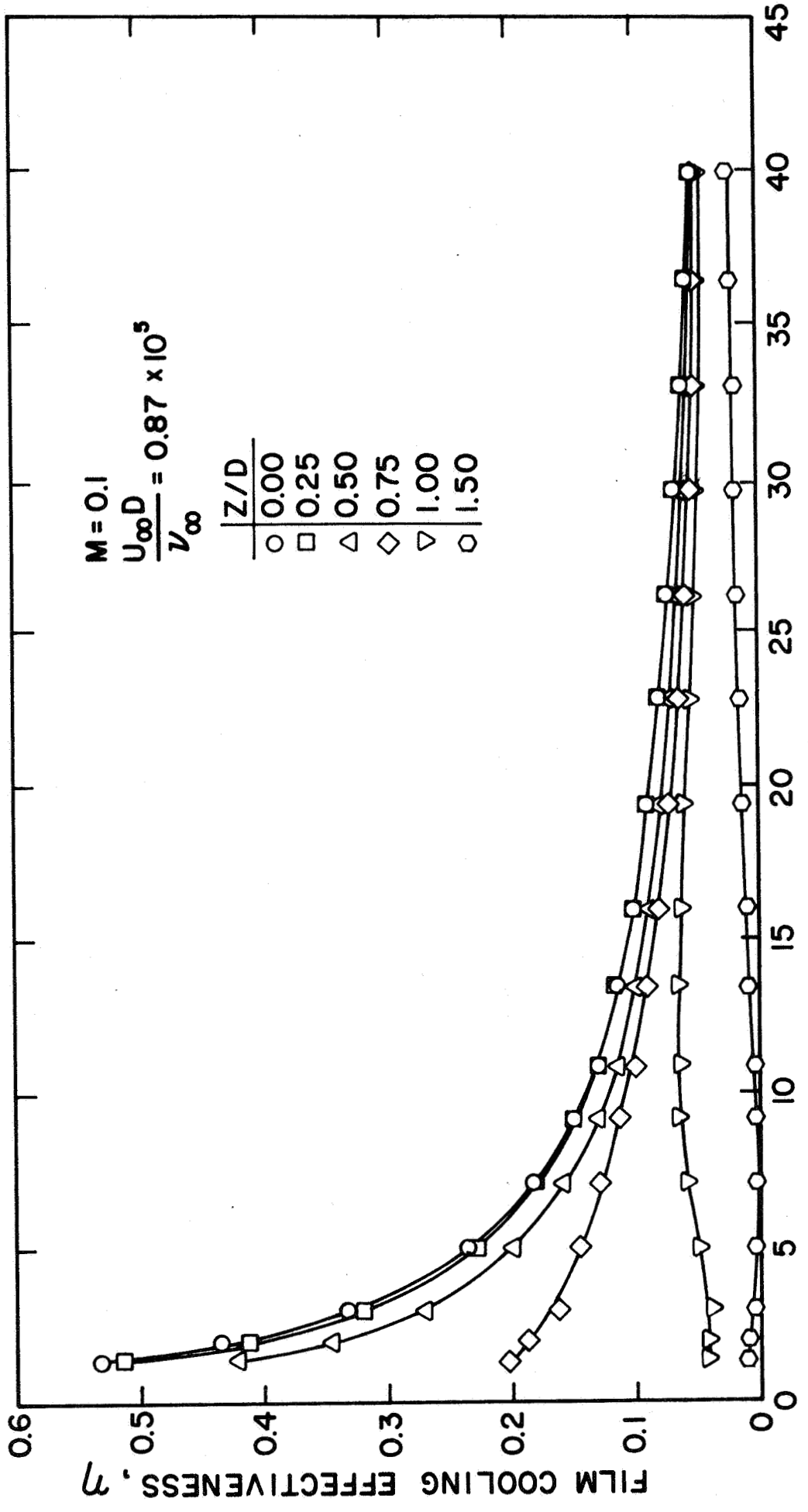

Fig. 19 Axial effectiveness distributions for 90^0 injection angle, M = 0.1

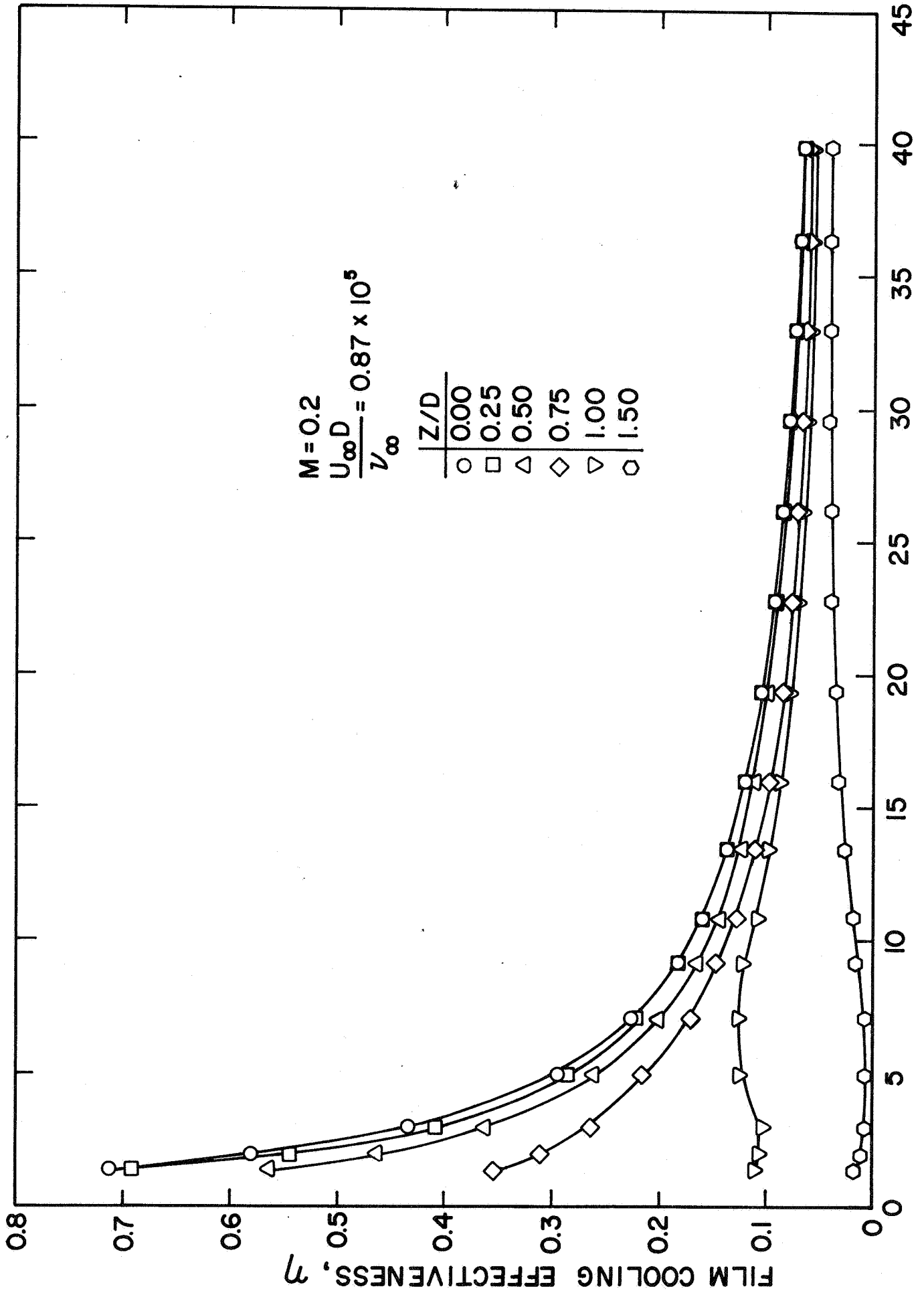

Fig. 20 Axial effectiveness distributions for 90° injection angle, M = 0.2

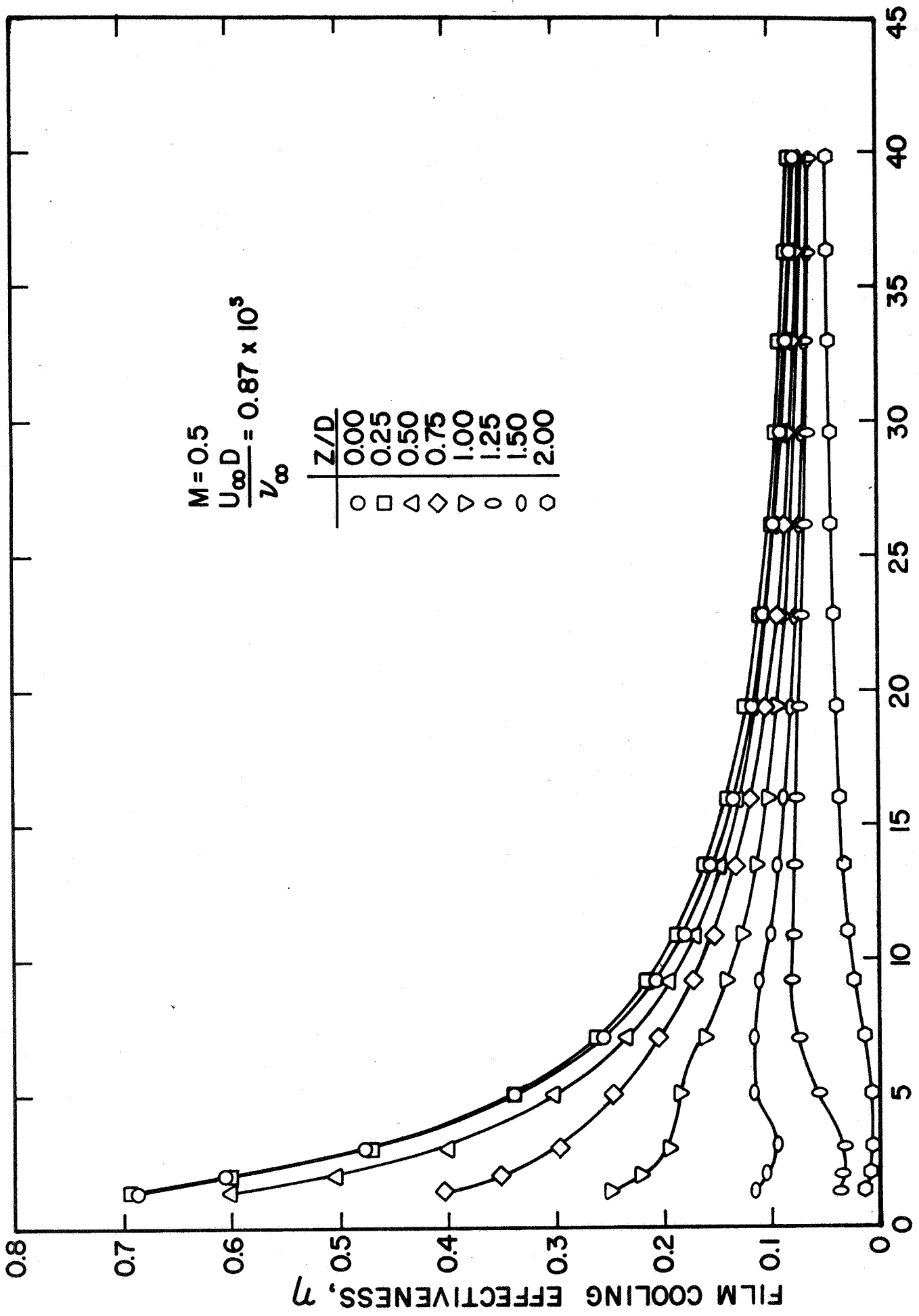

Fig. 21 Axial effectiveness distributions for 90^o injection angle, M = 0.5

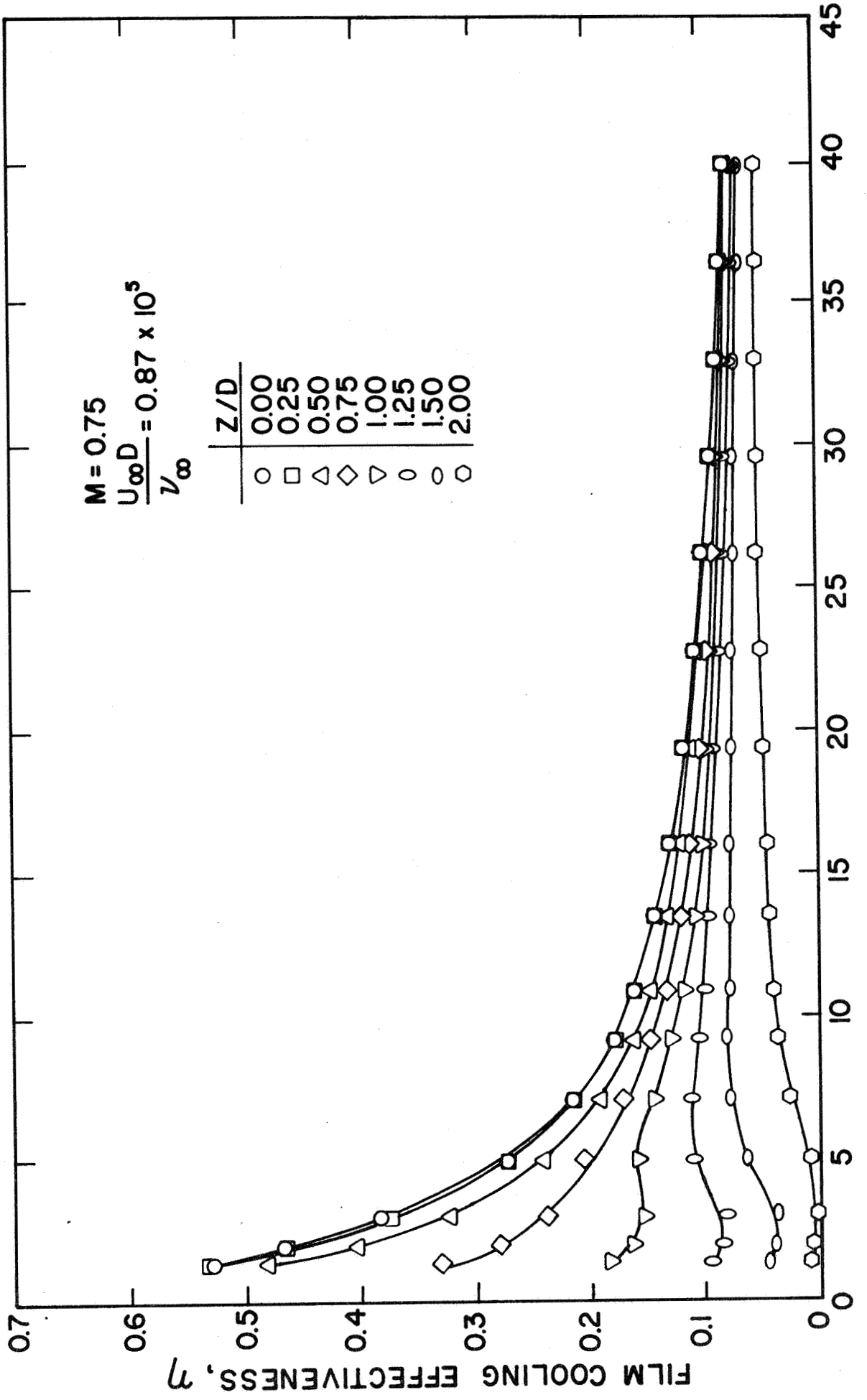

Fig. 22 Axial effectiveness distributions for 90° injection angle, M = 0.75

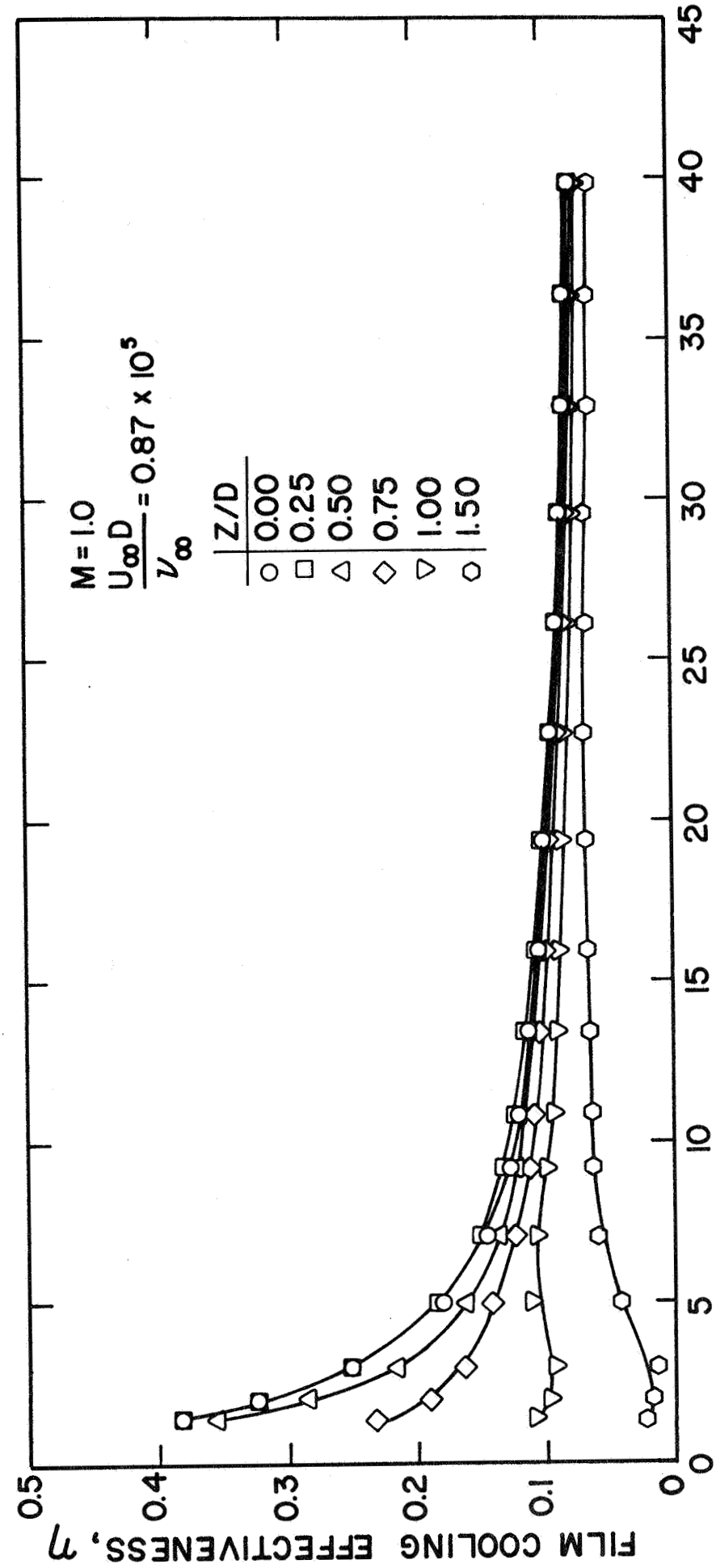

Fig. 23 Axial effectiveness distributions for 90° injection angle, M = 1.0

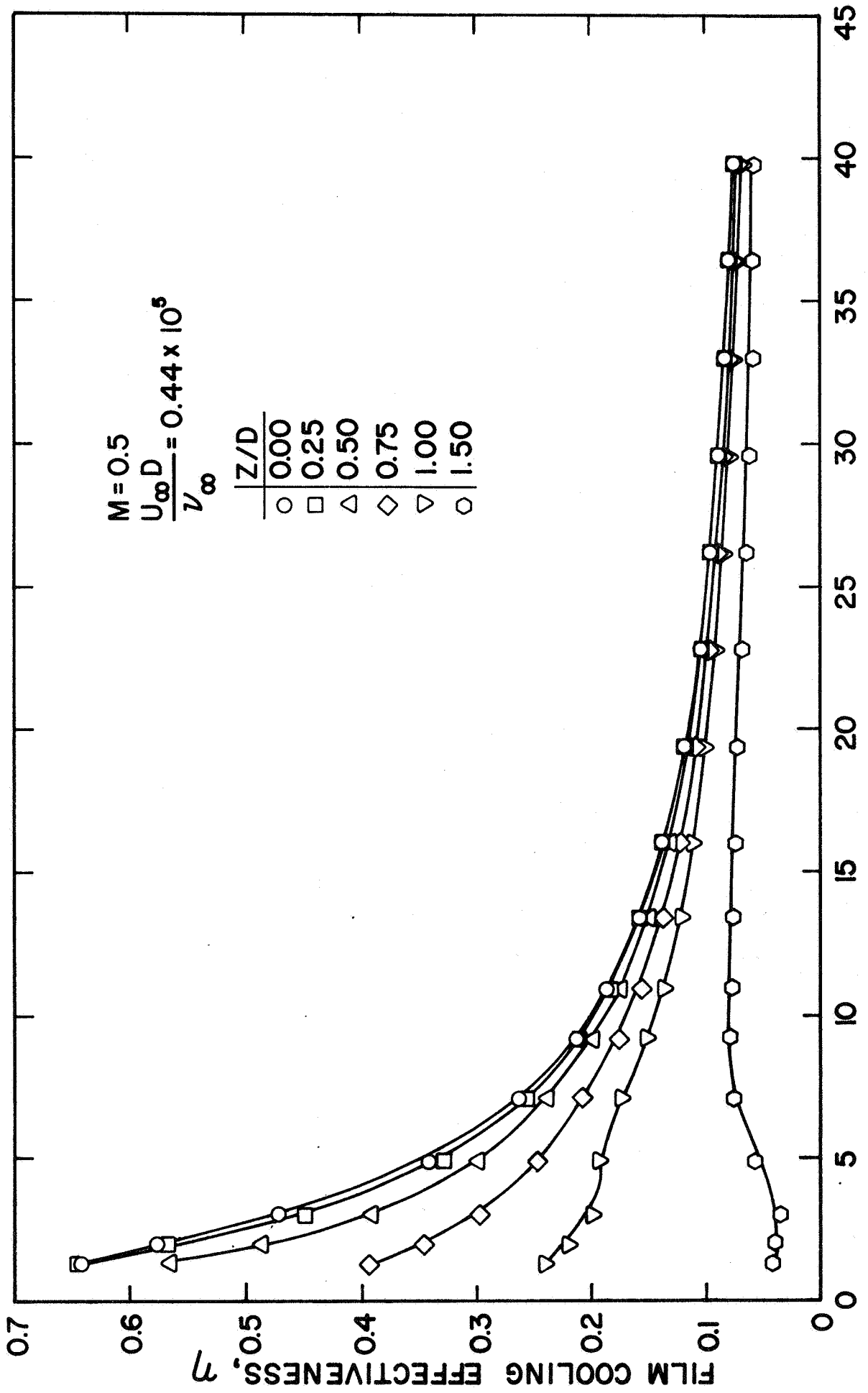

Fig. 24 Axial effectiveness distributions for 90^o injection angle, M = 0.5

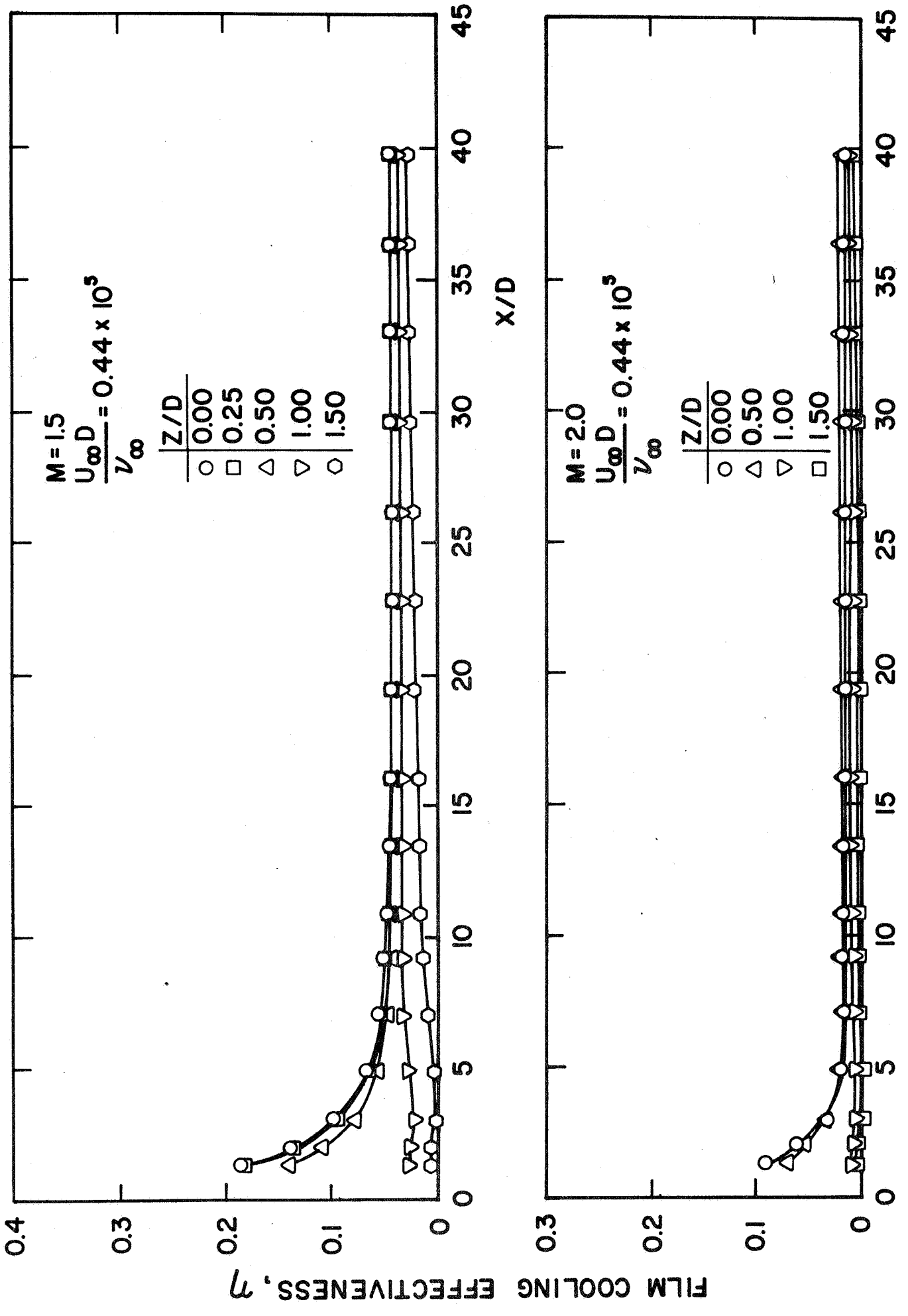

Fig. 25 Axial effectiveness distributions for 90^o injection angle, M = 1.5 and 2.0

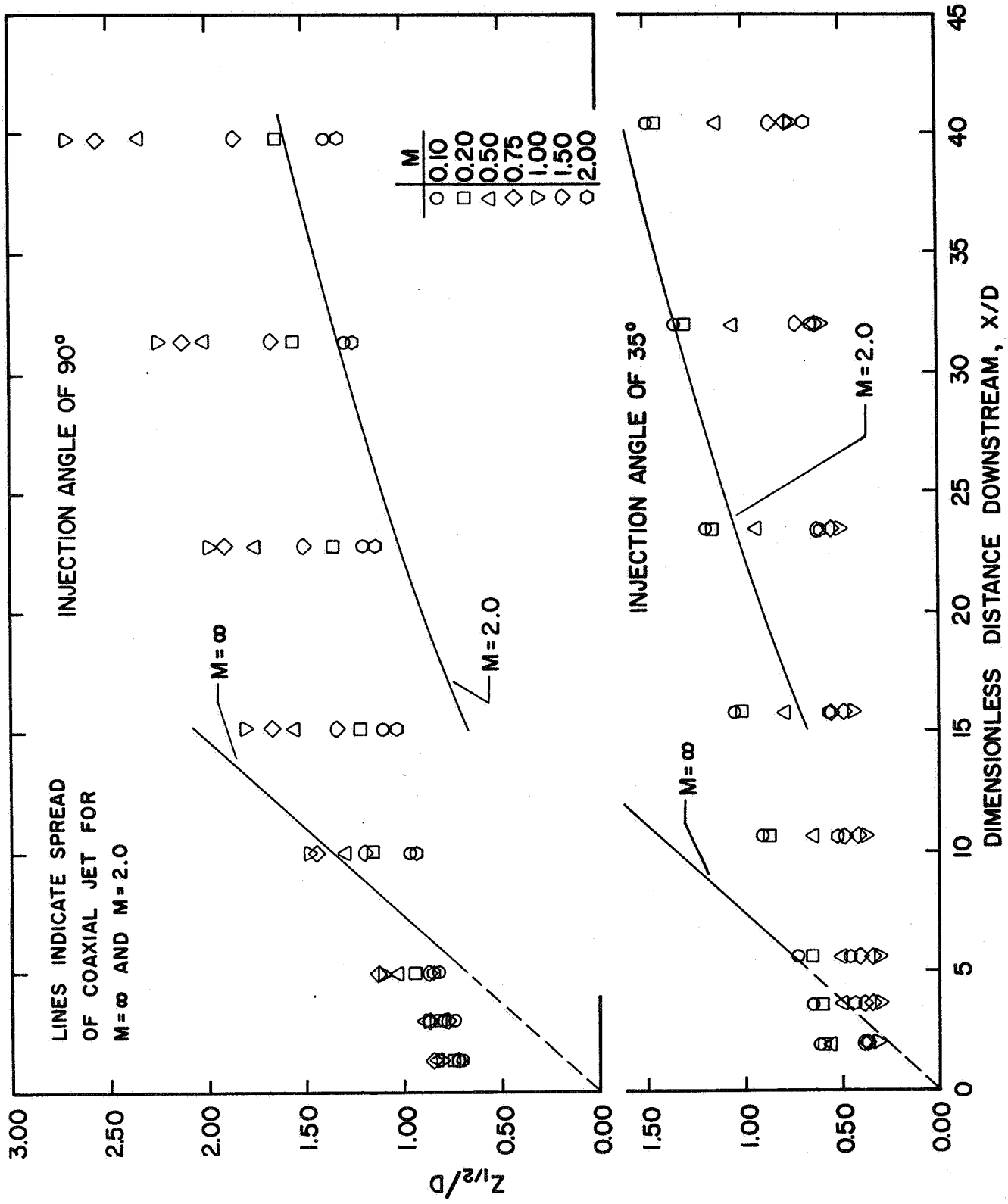

Fig. 26 Lateral spreading of injected fluid as determined from wall temperature distributions
Injection angles of 90^0 and 35^0

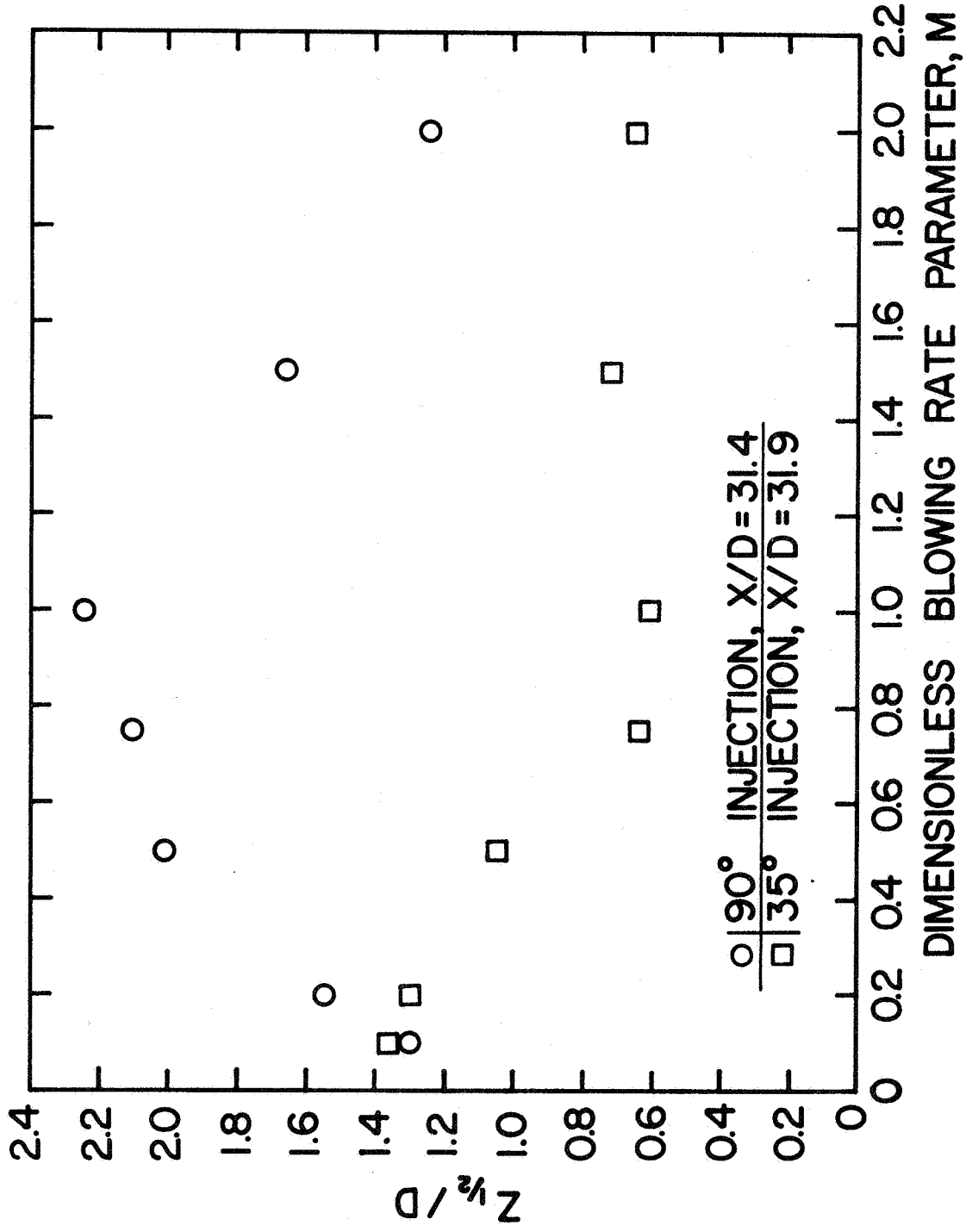

Fig. 27 The effect of the blowing rate parameter on the lateral spreading of injected fluid

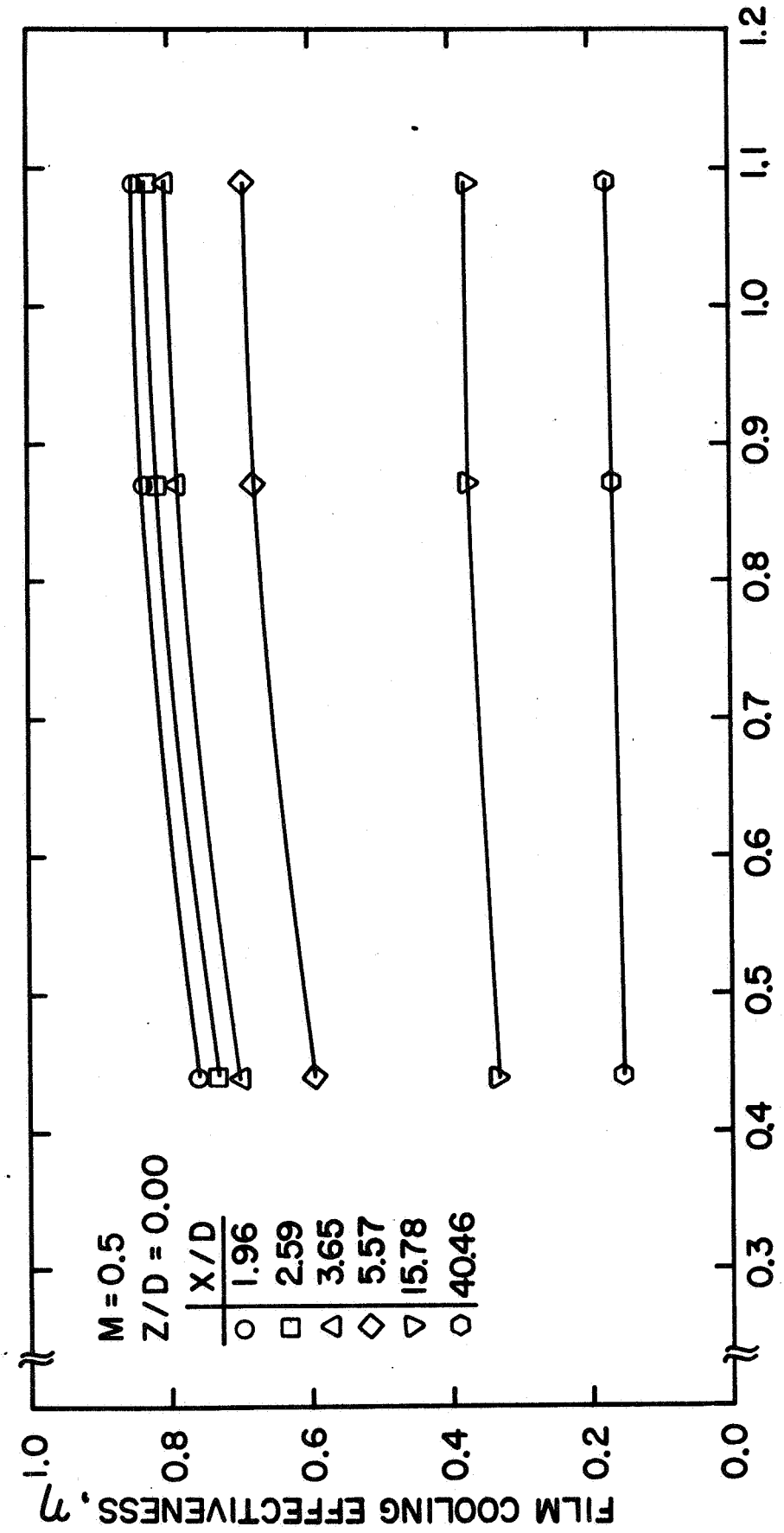

Fig. 28 Effect of $U_\infty D/\nu_\infty$ on film cooling effectiveness for injection at an angle of 35°, M = 0.5, $Z/D = 0.00$

NAS 3-7904
SUMMARY REPORT
DISTRIBUTION LIST

	ADDRESSEE	Mail Stop	NUMBER OF COPIES
1.	NASA-Lewis Research Center 21000 Brookpark Road Cleveland, Ohio 44135		
	Attention: Air-Breathing Engine Procurement Section	60-5	1
	Report Control Office	5-5	1
	Technology Utilization Office	3-19	1
	Library	60-3	2
	Fluid System Components Div.	5-3	1
	I. I. Pinkel	5-3	1
	W. L. Stewart	77-2	1
	P. Hacker	5-3	1
	J. Howard Childs	60-4	1
	Dr. W. H. Roudebush	60-6	1
	E. L. Warren	60-6	1
	J. B. Esgar	60-4	1
	F. S. Stepka	60-6	10
	R. O. Hickel	60-6	1
	H. Ellerbrock	60-4	6
	L. Maciose	60-6	1
	J. Livingood	60-6	1
	J. Lucas	6-1	1
2.	NASA Scientific & Technical Information Facility P.O. Box 33 College Park, Maryland 20740 Attention: NASA Representative RQT-2448		6
3.	FAA. Headquarters 800 Independence Avenue, S.W. Washington, D.C. 20546 Attention: Brig. General J. C. Maxwell		1
	F.B. Howard / SS120		1
4.	NASA Headquarters Washington, D.C. 20546 Attention: N.F. Rekos (RAP)		1
5.	Department of the Army U.S. Army Aviation Material Laboratory Fort Estis, Virginia 23604 Attention: John White		1

6. Headquarters
Wright-Patterson AFB, Ohio 45433
Attention: J. L. Wilkins, SESOS — 2

7. AFAPL (APTC)
Wright-Patterson AFB, Ohio 45433
Attention: Lt. D. R. Quick — 1

8. Air Force Office of Scientific Research
Propulsion Research Division
USAF Washington, D.C. 20025 — 1

9. Defense Documentation Center (DDC)
Cameron Station
5010 Duke Street
Alexandria, Virginia 22314 — 1

10. NASA-Langley Research Center
Langley Station
Technical Library
Hampton, Virginia 23365
Attention: Mark R. Nichols — 1
John V. Becker — 1

11. United Aircraft Corporation
Pratt & Whitney Aircraft Division
Florida Research & Development Center
P.O. Box 2691
West Palm Beach, Florida 33402
Attention: R. A. Schmidtke — 1

12. United Aircraft Corporation
Pratt & Whitney Aircraft Division
400 Main Street
East Hartford, Connecticut 06108
Attention: C. Andreini — 2
Library — 1

13. United Aircraft Research
East Hartford, Connecticut
Attention: Library — 1

14. Allison Division of GMC
Department 8894, Plant 8
P.O. Box 894
Indianapolis, Indiana 46206
Attention: J. N. Barney — 1
C. E. Holbrook — 1
Library — 1

15. Northern Research & Engineering Corporation
219 Vassar Street
Cambridge, Massachusetts 02139
Attention: K. Ginwala — 1

16. General Electric Company
Flight Propulsion Division
Cincinnati, Ohio 45215
Attention: J. W. McBride N-44 — 1
F. Burggraf H-32 — 1
S. N. Suciu H-32 — 1
C. Danforth H-32 — 1
Technical Information Center N-32 — 1

17. General Electric Company
1000 Western Avenue
West Lynn, Massachusetts 01905
Attention: Dr. C. W. Smith-Library Bldg. 2-40M — 1

18. Curtiss-Wright Corporation
Wright Aeronautical Division
Wood-Ridge, New Jersey 07075
Attention: S. Lombardo — 1

19. Air Research Manufacturing Company
402 South 36th Street
Phoenix, Arizona 85034
Attention: Robert O. Bullock — 1

20. Air Research Manufacturing Company
9851 Sepulveda Boulevard
Los Angeles, California 90009
Attention: Dr. N. Van Le — 1

21. AVCO Corporation
Lycoming Division
350 South Main Street
Stratford, Connecticut 06497
Attention: Claus W. Bolton — 1
Charles Kuintzle — 1

22. Continental Aviation & Engineering Corporation
12700 Kercheval
Detroit, Michigan 48215
Attention: Eli H. Benstein — 1
Howard C. Walch — 1

23. International Harvester Company
Solar Division - 2200 Pacific Highway
San Diego, California 92112
Attention: P. A. Pitt — 1
Mrs. L. Walper — 1

24.	George Derderian AIR 53622 B Dept. of Navy Bureau of Navy Washington, D.C. 20360		1
25.	The Boeing Company Commercial Airplane Division P.O. Box 3991 Seattle, Washington 98124 Attention: C. J. Schott	80-66	1
26.	Aerojet-General Corporation Sacramento, California 95809 Attention: M. S. Nylin Library Rudy Bear		1 1 1